#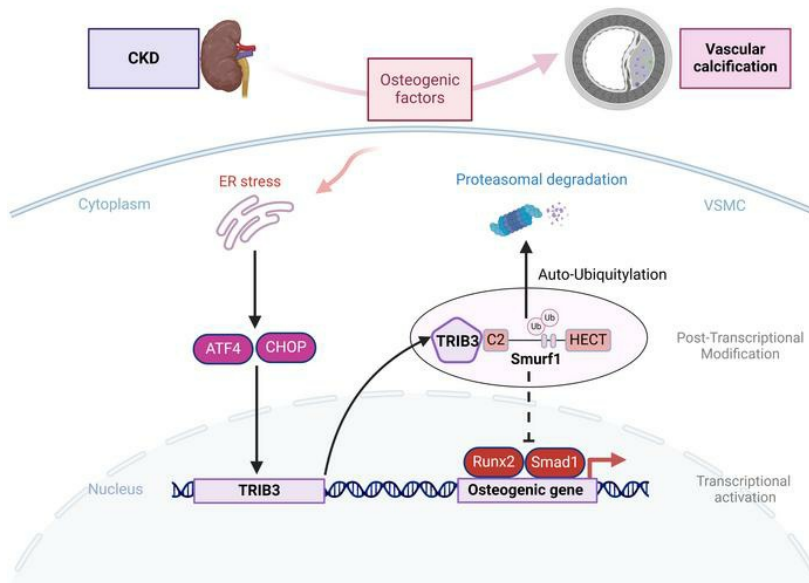 TRIB3 mediates vascular calcification through facilitating self-ubiquitination and dissociation of Smurf1 in chronic renal disease

Yihui Li, … , Hao Wang, Ming Zhong

Research   In-Press Preview   Cardiology   Vascular biology

Graphical abstract

TRIB3 mediates vascular calcification by facilitating self-ubiquitination and dissociation of Smurf1 in chronic renal disease

Yihui Li[1,2], Chang Ma[1], Yanan Sheng[1], Shanying Huang[1], Huaibing Sun[3], Yun Ti[1], Zhihao Wang[4], Feng Wang[5], Fangfang Chen[6], Chen Li[2], Haipeng Guo[2], Mengxiong Tang[7], Fangqiang Song[8], Hao Wang[2], Ming Zhong[1]

[1]State Key Laboratory for Innovation and Transformation of Luobing Theory; Key Laboratory of Cardiovascular Remodeling and Function Research of MOE, NHC, CAMS and Shandong Province; Department of Cardiology, Qilu Hospital of Shandong University, Jinan, China.

[2]Department of Critical Care Medicine, Qilu Hospital; Innovation Research Center for Sepsis and Multiple Organ Injury, Shandong University, Jinan, China.

[3]Department of Organ Transplantation, Qilu Hospital, Shandong University, Jinan, China.

[4]Department of Geriatric Medicine, Qilu Hospital, Shandong University, Jinan, China.

[5]Department of Critical Care Medicine, Shandong Provincial Hospital, Jinan, Shandong, China

[6]Department of Cardiology, Shandong Provincial Qianfoshan Hospital, Jinan, Shandong, China

[7]Department of Emergency, Qilu Hospital, Shandong University, Jinan, China.

[8]Department of Critical Care Medicine, the Affiliated Tengzhou Hospital of Xuzhou Medical University/ Tengzhou Central People's Hospital, Shandong

Authorship note: YL and CM contributed equally to this work and are co-first authors.

Address correspondence to: Ming Zhong, State Key Laboratory for Innovation and Transformation of Luobing Theory; Key Laboratory of Cardiovascular Remodeling and Function Research of MOE, NHC, CAMS and Shandong Province; Department of Cardiology, Qilu

Hospital of Shandong University, Jinan, China. Phone:86.531.82165801; E-mail: zhongming2sdu@163.com. Or Hao Wang, Department of Critical Care Medicine, Qilu Hospital; Innovation Research Center for Sepsis and Multiple Organ Injury, Shandong University, Jinan, China. Phone:86.531.82165060; E-mail: wanghao34@126.com.

Abstract

The osteogenic environment promotes vascular calcium phosphate deposition and aggregation of unfolded and misfolded proteins, resulting in endoplasmic reticulum (ER) stress in chronic renal disease (CKD). Controlling ER stress through genetic intervention is a promising approach for treating vascular calcification. In this study, we demonstrated a positive correlation between ER stress-induced tribble 3 (*TRIB3*) expression and progression of vascular calcification in human and rodent CKD. Increased *TRIB3* expression promoted vascular smooth muscle cell (VSMC) calcification by interacting with the C2 domain of the E3 ubiquitin-protein ligase Smurf1, facilitating its K48-related self-ubiquitination at Lys381 and Lys383 and subsequent dissociation from the plasma membrane and nuclei. This degeneration of Smurf1 accelerated the stabilization of the osteogenic transcription factors RUNX Family Transcription Factor 2 (Runx2) and SMAD Family Member 1 (Smad1). C/EBP homologous protein and activating transcription factor 4 are upstream transcription factors of *TRIB3* in an osteogenic environment. Genetic knockout of *TRIB3* or rescue of Smurf1 ameliorated VSMC and vascular calcification by stabilizing Smurf1 and enhancing the degradation of Runx2 and Smad1. Our findings shed light on the vital role of *TRIB3* as a scaffold in ER stress and vascular calcification and offer a potential therapeutic option for chronic renal disease.

Graphic abstract
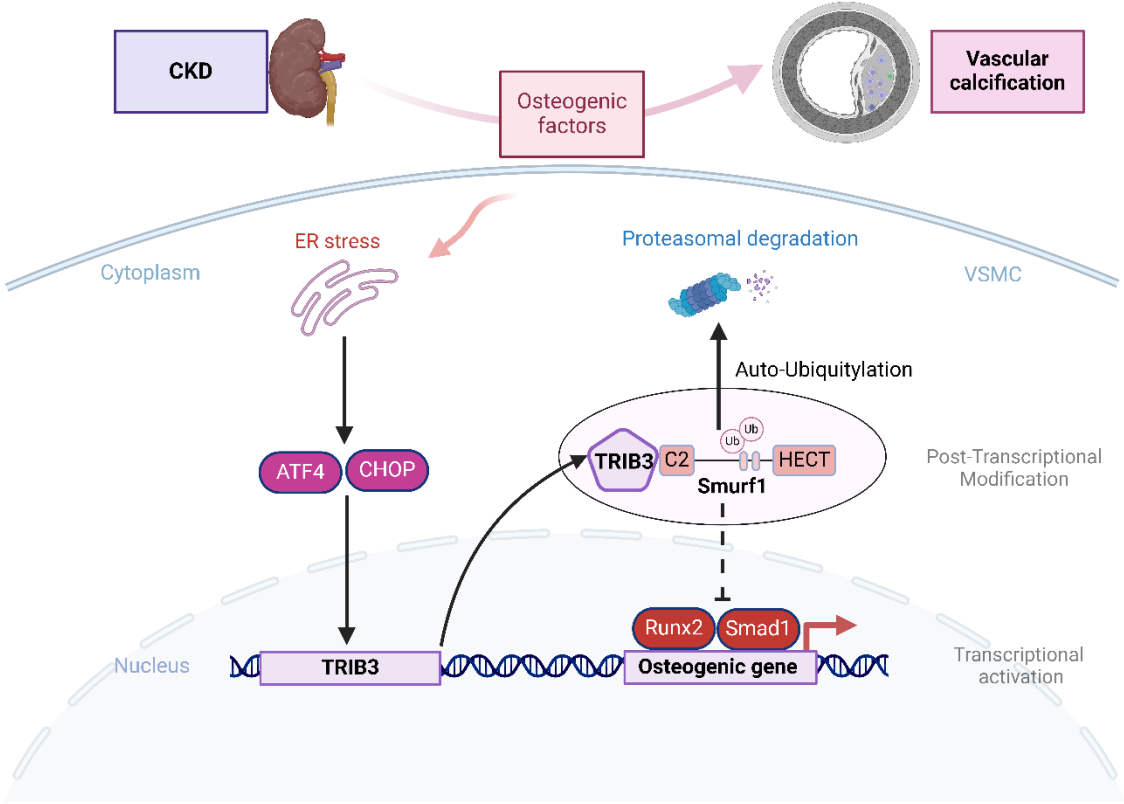
Created in BioRender.

Introduction

Vascular calcification, characterized by precipitation of hydroxyapatite mineral within the arterial wall, is an independent risk factor associated with cardiovascular diseases and cardiovascular mortality in both the general population and individuals with chronic kidney disease (CKD) (1). The prevalence of vascular calcification in CKD ranges from 47–92% (2, 3). In a significant number of patients with CKD, the size of coronary artery calcification is an independent risk factor and inversely correlated with estimated glomerular filtration rate (4). Traditional cardiovascular and CKD risk factors (diabetes, dyslipidemia, inflammation) (5) and related injury (phosphate retention, excessive calcium intake, and dialysis experience) (6) are associated with the severity and progression of vascular calcification.

Calcification occurs in the arterial intima and media, with vascular smooth muscle cell (VSMC) being key cell types involved in the calcification process (7). In normal adult tissues, VSMC exhibit a contractile phenotype characterized by a slow rate of proliferation and a predominant contractile function (8). Different from other muscle cells, VSMC cells do not terminally differentiate and display phenotypic plasticity (9). These cells can respond to local and systemic stress, altering their phenotype. In an osteogenic environment, such as high phosphate and bone morphogenetic protein (BMP), VSMC are capable of altering their gene expression profile, enhancing the expression of osteoblastic markers such as RUNX family transcription factor 2 (*Runx2*) and SMAD Family Member 1 (*Smad1*), and resembling osteoblasts or chondrocytes (10).

The endoplasmic reticulum (ER) is the first organelle involved in protein synthesis, where most secretory and transmembrane proteins fold and mature (11). ER stress occurs when the

accumulation of unfolded proteins exceeds the folding capacity of the ER, triggering the activation of the unfolded protein response (UPR) signaling pathway (12, 13). UPR and ER stress are prominently involved in various renal diseases, including primary glomerulonephritides (14), genetically associated glomerular diseases (15), diabetic nephropathy (16), acute kidney injury (AKI) (17), and CKD (18). In addition, it has been widely documented that ER stress can accompany vascular calcification in mice and rats (19). However, the mechanism linking vascular calcification and ER stress in CKD remains unclear.

Tribbles homolog 3 (*TRIB3*), a 45 kDa pseudokinase, was initially identified as a delayer of mitosis in *Drosophila* (20). Recently, *TRIB3* has been proven to be ER stress and metabolic sensor involved in glucose and lipid metabolism and contributes to diabetes and related cardiovascular diseases (21). Our group found insulin resistance and other ER stress markedly unregulated *TRIB3*, which serves as a scaffold for Akt and mitogen-activated protein kinases (MAPKs) (22). Data in our (22, 23) and other previous studies (24) proved that *TRIB3* expression is increased by CKD. Silencing *TRIB3* alleviates diabetic atherosclerosis (24) and nephropathy (24). However, the role of *TRIB3* in CKD-related vascular calcification remains unclear.

Results

Elevation of TRIB3 expression and ER stress during calcifying conditions

To investigate the effects of known osteogenic differentiation and ER stress triggers in VSMC on vascular TRIB3 expression, we conducted a series of in vitro experiments. As shown in Figure 1A and 1B, treatment with phosphate (Pi), high glucose plus insulin, high glucose, recombinant BMP2 protein, ox-LDL, and the ER stress agonist tunicamycin substantially upregulated TRIB3

protein expression and mRNA transcription in human VSMC (hVSMC). These effects were paralleled by increased protein expression of ER stress markers (glucose-regulated protein 78 (GRP78) and phosphorylation of protein kinase R-like endoplasmic reticulum kinase (PERK)), but were abolished by the ER stress antagonist 4-Phenylbutyric acid (4PBA). Further experiments were conducted to investigate TRIB3 expression in humans under uremic conditions. As shown in Supplementary Figure 1A, TRIB3 and ER stress markers was markedly upregulated following treatment with uremic sera (Supplementary Table 1).

In human arterial specimens (Supplementary Table 2-4), atherosclerosis of the coronary and carotid arteries is represented by intimal layer calcification, whereas medial calcification occurs in the aorta. The mRNA expression of *TRIB3* was higher in the carotid, renal and coronary arteries of patients with CKD compared to subjects with normal kidney function (Figure 1C-D and Supplementary Figure 1B). More critically, TRIB3 mRNA transcription and protein expression in different arteries of patients with CKD was substantially correlated with calcium deposition (Figure 1E, F, and Supplementary Figure 1C-E). Furthermore, TRIB3 protein levels were substantially elevated in renal artery samples from patients with CKD compared with individuals with normal renal function, and TRIB3 expression positively correlated with ER stress markers (Figure 1G, Supplementary Figure 1F-G).

As demonstrated by histological examination, the TRIB3 protein levels and the osteogenic marker osteopontin (OPN) were elevated in the calcified intima and media of human arteries in CKD patients compared to the control group, and were confined to the calcified arterial regions (Figure 1H and Supplementary Figure 1H-I).

Furthermore, in mouse CKD models derived from acute kidney injury (unilateral ureteral

obstruction (UUO) mice, 5/6 nephrectomy (Nx) mice) and chronic metabolic disturbance-related

CKD (db/db mice, apolipoprotein E (*ApoE*) knockout with streptozotocin (STZ) administration

mice), *TRIB3* mRNA expression in the aorta was substantially higher than that in Sham or WT

mice (Supplementary Figure 1J-M).

TRIB3 Suppresses Runx2 and Smad1 Degradation in VSMC

To investigate TRIB3 downstream biological functions and signaling pathways involved in

VSMC calcification, we assessed the transcriptomes of hVSMC treated with *TRIB3* siRNA and

primary mouse VSMC (mVSMC) derived from *TRIB3* knockout mice using bulk RNA-seq.

Gene Ontology (GO) analysis revealed that *TRIB3* was involved in bone remodeling and

ubiquitin-dependent protein catabolic processes, except for classical metabolism regulation and

the MAPK pathway in hVSMC and mVSMC (Figure 2A-B and Supplementary Figure 2A-B).

These data suggested that *TRIB3* participates in the regulation of osteogenic transcription factors

and ubiquitination. To identify upstream molecules associated with DEGs after *TRIB3* knockout,

transcription factor-binding signature analysis in KnockTF2.0 (25) was performed and

overlapped with DisGenNet C0342649. We found that the functions of the osteogenic

transcription factors *Runx2* and *Smad1* were downregulated after *TRIB3* knockout (Figure 2C).

To validate the function of these osteogenic transcription factors in the elevation of *TRIB3*

expression by simulating an osteogenic environment, *TRIB3* adenovirus was transfected into

hVSMC. Unexpectedly, *TRIB3* overexpression did not affect the transcription factors *Runx2*,

Smad1, *Sox2*, Msh Homeobox 2 (*Msx2*), the classical osteogenic Kruppel-like factor 6 (*Klf6*), or

Twist Family BHLH Transcription Factor 1 (*Twist1*) transcript levels (Figure 2D). However,

TRIB3 overexpression increased Runx2 and Smad1 protein levels (Figure 2E). This suggests that

TRIB3 regulates Runx2 and Smad1 protein levels posttranslationally.

Subsequently, we evaluated the stability of Runx2 and Smad1 using the proteasome inhibitor MG132 and the protein synthesis inhibitor cycloheximide (CHX). Runx2 and Smad1 protein levels substantially decreased in hVSMC treated with CHX, and MG132 attenuated this effect , phosphate treatment and *TRIB3* overexpression had an effect similar to that of MG132 in blocking Runx2 and Smad1 turnover (Figure 2F-K). Thus, Runx2 and Smad1 are rapidly degraded through the proteasomal pathway in VSMC. TRIB3 might increase Runx2 and Smad1 protein accumulation by suppressing proteasomal degradation in response to osteogenic stimuli.

TRIB3 Promotes Runx2 and Smad1 Ubiquitination via Interacting with Smurf1

Although *TRIB3* suppresses proteasomal degradation of Runx2 and Smad1, TRIB3 does not belong to any of the ubiquitination or deubiquitination enzyme families. E3 ubiquitin ligases are crucial for catalyzing the ubiquitination and facilitating the transfer of ubiquitin (26). Therefore, we examined whether TRIB3 regulates Runx2 and Smad1 via intermediary E3 ubiquitin ligases. We identified that *Runx2* and *Smad1* shared common E3 ubiquitin ligases, Smad ubiquitination regulatory factor 1 (Smurf1), in humans and mice via the Ubibrowse 2.0, comprehensive protein motif, motif analysis, protein GO, and network annotation (Figure 3A). Because Smurf2 derived from the same family also showed high scores, we separately transfected exogenous Smurf1 and Smurf2 into hVSMC overexpressing *TRIB3*. The results revealed that only Smurf1 could reverse the increase in Runx2 and Smad1 proteins induced by TRIB3 (Figure 3B). Indeed, TRIB3 deficiency in human or mouse VSMC resulted in endogenous smurf1 accumulation in response to phosphate stimuli (Figure 3C).

Smurf1 belongs to the neural precursor cell-expressed developmentally downregulated

protein 4 (NEDD4) subfamily, regulates ligase activity-independent self-ubiquitylation (27). In addition, TRIB3 time-dependently increased endogenous smurf1 self-ubiquitination and proteasomal turnover in hVSMC (Figure 3D). And knockdown *TRIB3* could decrease endogenous smurf1 self-ubiquitination (Figure 3D). To confirm this finding, we transfected exogenous *TRIB3* and *Smurf1* into HEK293T cells，which confirmed the regulatory effect of TRIB3 on Smurf1 ubiquitination (Figure 3E). A mutant of TRIB3 238-266aa was used to confirm the interaction site with Smurf1 (Figure 3F), as reported previously (28). It was confirmed that TRIB3 promoted Smurf1 self-ubiquitination via K48 linked ubiquitination, but not K63 (Figure 3F). Multiple sequence alignment and ubiquitination site prediction indicated that TRIB3-mediated K48-linked ubiquitination may occur at the highly conserved K381 and K383 sites of Smurf1 (Figure 3G). We then created a Smurf1 mutant where a lysine residue was substituted with arginine and assessed the polyubiquitination level of this mutant in HEK293T cells. In cells expressing Smurf1 whose K381R or K383R (residue was replaced) the effect of TRIB3 on accelerating Smurf1 ubiquitination was attenuated (Figure 3H).

TRIB3 interacted Smurf1 and promoted its self ubiquitination through C2 domain

TRIB3 exerts various effects through interactions with other proteins (29). Previous study (28) identified amino acids 238–266 of TRIB3 as key regions interacting with Smurf1. Nonetheless, the domain that Smurf1 interacted with TRIB3 remains unclear. Using molecular docking and deletion mutants of the Smurf1 domain, we observed that TRIB3 interacts with the C2 domain of Smurf1 (Figure 4A-C). In the molecular dynamics simulations performed using Gromacs, the TRIB3 and Smurf1 complex remained stable, as indicated by the stable root mean square deviation (RMSD) after 20000 ps of simulation, suggesting a slow but stable interaction between

TRIB3 and Smurf1 (Supplementary Figure 3A). Additionally, upon binding, the homologous to

the E6-AP Carboxyl Terminus (HECT) domain of Smurf1 exhibited conformational unfolding

(Supplementary Movie), indicated by two low energy regions in the Energy Landscape

(Supplementary Figure 3B). Through surface plasmon resonance (SPR), the equilibrium

dissociation constant (KD) between the two recombinant proteins was determined to be 1.03×10^{-6}M (Supplementary Figure 3C). Given that the C2 domain is crucial for Smurf1 localization to

the plasma membrane (28), we investigated whether the subcellular localization of Smurf1 is

affected by its interaction with TRIB3. Endogenous Smurf1 was localized in whole cells from the

plasma membrane to the nucleus, but exogenous TRIB3 resulted in Smurf1 dissociation from the

plasma membrane and nucleus and conglomeration in the cytoplasm. Transfection with

exogenous full-length *Smurf1* (Smurf1 WT) alleviated TRIB3 induced dissociation from the

plasma membrane and nucleus, and some Smurf1 was localized to the plasma membrane and

nucleus. However, the mutant Smurf1 lacking C2 domain (Smurf1 ΔC2) showed none of these

effects (Figure 4D). Additional cellular fractionation by western blotting yielded similar results

(Figure 4E). Furthermore, exogenous TRIB3 did not induce the promotion of ubiquitination for

Smurf1 ΔC2 in HEK293T cells, and exogenous Smurf1ΔC2 did not reverse TRIB3-induced

elevation of Runx2 and Smad1 (Figure 4F). Additionally, we verified that the introduction of

exogenous Smurf1 WT successfully reversed the accelerated calcification of hVSMC induced by

TRIB3. However, Smurf1 ΔC2 had no such effect (Figure 4G).

Our data collectively demonstrated that TRIB3 interacts with the Smurf1 C2 domain to

promote its dissociation from the plasma membrane and nucleus, translocate into the cytoplasm

for self-ubiquitination, and promotes calcification in VSMC.

ATF4 and CHOP induced TRIB3 transcription in phosphate stimuli

To investigate the mechanism underlying the increased transcription and expression of TRIB3 in response to phosphate-induced calcification, we initially reanalyzed the published data GSE35681 and confirmed the significant enrichment of ATF4 and CHOP in the same *TRIB3* promoter region under ER stress conditions in mouse embryonic fibroblasts. Moreover, ATF4 and CHOP shared highly similar sequences (Figure 5A). Therefore, we constructed a *TRIB3* promoter reporter luciferase plasmid and related core binding site mutant plasmids (*TRIB3*-WT and *TRIB3*-mut) (Figure 5B). Phosphate substantially boosted luciferase activity from the *TRIB3*-WT promoter-reporting plasmid but had no effect on *TRIB3*-mut. Additionally, ATF4 and CHOP knockdown effectively reduced or eliminated the phosphate-induced increase in luciferase activity, respectively (Figure 5C).

After ER stress stimulation, mVSMC exhibited increased binding of the *TRIB3* promoter to ATF4 and CHOP, as determined by ChIP-PCR in phosphate-treated cells (Figure 5D). Formaldehyde-Assisted Isolation of Regulatory Elements (FAIRE)-PCR confirmed the binding of ATF4 and CHOP to the open chromatin region of the *TRIB3* promoter (Figure 5E-F).

Furthermore, the ER stress inhibitor 4PBA suppressed the upregulation of TRIB3 caused by phosphate while simultaneously inhibiting the transcription of *ATF4* and *CHOP* (Figure 5G). Additionally, the knockdown of *ATF4* and *CHOP* attenuated the phosphate-induced increase in TRIB3 expression (Figure 5H, I). To confirm that the upregulation of TRIB3 was driven by ER stress, we treated mVSMC with the ER stress agonist tunicamycin, which yielded similar results (Supplementary Figure 4).

Taken together, these findings indicate that phosphate promotes the transcriptional

upregulation of *TRIB3* via the facilitation of ATF4 and CHOP binding, potentially serving as a mechanism for the promotion of TRIB3 expression in a calcified environment.

Effect of TRIB3 deficiency on ER-induced osteogenic differentiation of primary aortic smooth muscle cells

To further investigate the function of *TRIB3* in the osteogenic differentiation and calcification of VSMC under ER stress conditions, hVSMC and mVSMC were differentiated in phosphate combined with high glucose plus insulin, high glucose, recombinant BMP2 protein, ox-LDL, tunicamycin and 4PBA. Through shRNA silencing of *TRIB3* in hVSMC or knockout of *TRIB3* in mVSMC, both exhibited resistance to ER stress-induced calcification compared to control shRNA-treated hVSMC or WT mVSMC (Figure 6A-D). Furthermore, the downstream calcification factors of Runx2 and Smad1, including Bone Gamma-Carboxyglutamate Protein (*BGLAP*), tissue-nonspecific alkaline phosphatase (*ALPL*), *BMP2*, and Collagen type I alpha 1(*COL1A1*) were upregulated in response to phosphate stimulation in hVSMC. Importantly, this upregulation was reversed by the deficiency of *TRIB3* (Figure 6E).

Effect of TRIB3 deficiency during AKI–induced CKD vascular calcification in mice

To assess the in vivo relevance of *TRIB3* in medial vascular calcification, experiments were conducted in *TRIB3* KO mice (*TRIB3* KO) and corresponding WT mice in a mouse model of CKD after AKI. After 12 weeks of right cortical electrocautery and left total nephrectomy, plasma urea was 2-3 fold elevation in both *TRIB3* KO and WT mice compared to the sham group (Supplementary Table 5). As shown by Alizarin red staining, and quantification of aortic calcium content, CKD mice showed severe aortic calcification. *TRIB3* knockout reduced calcification in the aorta of CKD mice (Figure 7A-D). In contrast, the aortic pulse wave velocity (PWV), an

indicator of vascular rigidity, increased in CKD mice, but the PWV elevation effect was blunted in *TRIB3* KO mice (Figure 7E). For ex vivo vascular mechanical index, wall tension was substantially increased in the aortic rings of 6 weeks CKD mice. *TRIB3* KO mice developed less wall tension after mechanical stretch than aortic rings from WT CKD mice (Figure 7F). The expression of the osteogenic transcription factors Runx2 and Smad1 increased in the aortic tissue of CKD mice, and these effects were substantially diminished in *TRIB3* KO mice (Figure 7G–H).

Additionally, we examined female CKD mice after AKI, and the results indicated that the above mechanisms are applicable to female individuals (Supplementary Figure 5). Using mouse models with vascular endothelial- or smooth muscle cell-specific *TRIB3* knockout, we observed that *TRIB3* knockout in smooth muscle cells resulted in a marked decrease in vascular calcification. In contrast, endothelial cell-specific *TRIB3* knockout mice did not exhibit this phenotype (Supplementary Figure 6).

Taken together, these data indicate that vascular smooth muscle cell *TRIB3* promotes vascular tunica media calcification and stiffness by supporting Smad1 and Runx2 protein stability in a mouse model of CKD after AKI.

Effect of TRIB3 deficiency on vascular calcification induced by metabolic CKD in mice

CKD-derived diabetes and other chronic metabolic diseases are widely recognized. Further experiments were conducted to examine the impact of *TRIB3* deficiency in a clinically relevant model of metabolic renal failure. A model of CKD combined with diabetes and hyperlipidemia was developed to investigate the role of *TRIB3* in metabolic CKD. Subtotal nephrectomy and STZ, combined with a diabetic diet, caused uremia in *ApoE* KO mice and in double-knockout *TRIB3* and *ApoE* mice (*ApoE*/*TRIB3* KO) (Supplementary Table 5). Histological staining

confirmed podocyte injury and fibrosis in CKD model-related hyperlipidemia and hyperglycemia (Supplementary Figure 7). Calcium nodule formation substantially increased in the aortic roots of CKD mice, indicating intimal vascular calcification (Figure 8A). Similarly, in CKD after AKI, *TRIB3* knockout substantially decreased calcium disposition in the aorta and aortic roots of patients with metabolic CKD (Figure 8A-D). Furthermore, metabolic CKD substantially upregulated PWV (Figure 8E), and *TRIB3* knockout substantially decreased these effects, although no significant difference was detected in arterial blood pressure among the groups of mice (Supplementary Table 5). In metabolic CKD mice, the expression of Smurf1 was suppressed, whereas the levels of Runx2 and Smad1 increase in the aortic roots. However, in *TRIB3* KO mice, these effects were improved (Figure 8F-G). To exclude the potential impact of *ApoE* knockout, we investigated the effects of *TRIB3* knockout alone on metabolic diabetic CKD model. Our findings demonstrate that *TRIB3* knockout alleviates vascular calcification in diabetic metabolic CKD mice, showing similar results to the *ApoE* knockout metabolic CKD model (Supplementary Figure 8). Thus, *TRIB3* deficiency protects against vascular intimal calcification in metabolic CKD.

Discussion

TRIB3 is a crucial scaffold protein contributed to the regulation of cellular stress, differentiation, and glucose-lipid metabolism. Previous studies have implicated *TRIB3* signaling in diabetic nephropathy and atherosclerotic vascular diseases. However, its role in the progression of vascular calcification in CKD is insufficiently elucidated. This study sheds light on the

involvement of VSMC *TRIB3* as a sensor of ER stress during CKD-associated vascular disease progression, leading to the enhanced stabilization of osteogenic transcription factors and subsequent vascular calcification.

Vascular calcification plays a significant role in cardiovascular mortality, and poses a greater threat to patients with CKD and atherosclerotic plaques in arteries (7). Increasing evidence suggests that CKD-related risk factors and complications such as insulin resistance, dyslipidemia, hypercalcemia, and hyperphosphatemia impose cellular stress, triggering UPR and ER stress (19). However, the current state of research fails to elucidate the unification of diverse calcification factors in CKD, specifically, how they collectively converge through ER stress to induce vascular calcification. Our study introduces *TRIB3* as a pivotal scaffold protein at the intersection of ER stress and ubiquitination, thereby establishing a paradigm connecting CKD-associated ER stress with the ubiquitination of various calcification factors, ultimately leading to vascular calcification.

Some patients with vascular calcification do not have CKD. To explore the role of *TRIB3* in the absence of CKD, we employed a high-dose Vitamin D3 injection model to simulate acute vascular calcification induced by elevated calcium and phosphate. The results also indicated that *TRIB3* substantially attenuates Vitamin D3-induced vascular calcification (Supplementary Figure 9). These findings suggest the broader role of *TRIB3* in modulating vascular calcification.

During ER stress, GRP78 dissociates from the ER, subsequently activating downstream transcription factors ATF4 and CHOP through phosphorylation or transcriptional mechanisms (19). Our reanalysis of CHOP and ATF4 ChIP-seq data indicated that *TRIB3* is a shared target gene of CHOP and ATF4. Further data confirmed that osteogenic conditions induced ER stress in VSMC, resulting in increased *TRIB3* transcription driven by CHOP and ATF4, highlighting

the important role of *TRIB3* as an effector in ER stress triggered by CKD in osteogenic environments.

TRIB3 functions as a pseudokinase during the integrated stress response, directly binding to the 'Thr-308' phosphorylation on AKT1 and inhibiting its activation (30). On the other hand, *TRIB3* can interact with ubiquitin protein binding ligases to regulate the stability of substrate proteins (30, 31). In our study, transcriptomic data suggested that *TRIB3* regulates the ubiquitination process in VSMC. Further experiments confirmed that *TRIB3* promotes the ubiquitination of Smurf1 in osteogenic environments. This finding is consistent with previous results in Cos7 (monkey kidney fibroblast-like cells) (28), but contrary to the results observed in the MDA-MB-231 cell line (human breast cancer cell line) (27). These results indicate that the regulation of E3 ubiquitin ligase activity by *TRIB3* may exhibit cell selectivity.

A previous study found *TRIB3* interaction with the Smurf family: *TRIB3* interacts with Smurf2, triggering the degradation of SMAD3 (32) and *TRIB3* dissociates from bone morphogenetic protein receptor II and triggers degradation of Smurf1 (28). We confirmed the direct interaction between TRIB3 and Smurf1, as well as the promotion of self-ubiquitination in human and mouse VSMC. Several studies have documented the involvement of Smurf1-mediated K48- and K63-linked polyubiquitination (33). K48-linked ubiquitination promotes substrate protein degradation by the proteasome, whereas K63-linked polyubiquitin chains participate in proteasome-independent mechanisms (33). Using VSMC, we demonstrated that TRIB3-mediated self-ubiquitination of Smurf1 in CKD occurs through a K48-dependent proteasomal pathway. Moreover, *TRIB3* accelerated Smurf1 self-ubiquitination with K48-linked ubiquitin chains at Lys381 and Lys383, resulting in enhanced translocalization and protein degeneration.

The self-ubiquitination level and intracellular localization of Smurf1 are modulated by the ER stress sensor *TRIB3*. Smurf1, composed of a C2 domain, two WW domains, and a HECT domain, is a critical regulator of TGFβ and BMP signaling (34). The C2 domain of Smurf1, interacts with the HECT domain of another Smurf1, and forms homodimers thereby inhibiting its self-ubiquitination (35, 36). In fact, our study revealed that TRIB3 interact with the C2 domain of Smurf1, and molecular simulations speculated that TRIB3 bind Smurf1 C2 and lift the HECT domain, triggering self-ubiquitination of Smurf1.

The Smurf1 C2 domain, known as the lipid-binding domain, is not only localized to the plasma membrane but also at negatively charged intracellular sites, serving as a selective binding domain (27). The C2 domain of Smurf1 exhibits substrate selection and cellular localization. Substrates of Smurf1 are localized to the plasma membrane (e.g., TGF-beta receptors and RhoA), cytoplasm (Smad1/5, MEKK2), or nucleus (Smad1/5, JunB and Runx2) (37). Immunofluorescence studies demonstrated that TRIB3 binding to Smurf1 induced by phosphate treatment or plasmid transfection resulted in Smurf1 detachment from the plasma membrane and nucleus, and then occur cytoplasmic aggregation. This dissociation of Smurf1 caused by *TRIB3* may be one of the reasons for the altered ubiquitination levels of Smurf1 substrates such as Smad1 and Runx2. RhoA and Axin1, substrates of Smurf1 and part of the Wnt pathway, are linked to vascular calcification (38). However, *TRIB3* knockout did not substantially reduce Wnt signaling during calcification (Supplementary Figure 10), suggesting that its role in this pathway requires further study.

ER stress is an active response of renal and vascular cells to survival stress (39). The emergence during evolution of pseudokinases, such as *TRIB3* act as scaffolding protein, inhibit

the 'real kinase' activity, assists cells in accomplishing complex functional transformations in the face of survival stress, including inhibiting proliferation, reducing protein synthesis and increasing protein degradation (40). Either the need for renal repair after AKI or the need for metabolic transformation of the kidney in chronic metabolic disease drives cellular ER stress (18, 40). However, persistent calcification stimuli in CKD result in sustained expression of TRIB3 in VSMC turning on the additional function of *TRIB3* to accelerate Smurf1 ubiquitination, leading to irreversible differentiation of VSMC towards osteoblast and ultimately resulting in vascular calcification.

In conclusion, our data indicate that *TRIB3*, an ER stress sensor in VSMC, tightly regulates the intracellular localization of the E3 ubiquitin ligase Smurf1 and its K48-related self-ubiquitination, subsequently controlling the transcription factor stability of Runx2 and Smad1. *TRIB3* acts as a scaffold molecule between ER stress and specific ubiquitin-mediated degradation of calcification transcription factors in CKD. Inhibition of TRIB3 may represent a potential strategy to counteract vascular calcification associated with CKD.

Methods

Sex as a biological variable. Our study examined male and female animals, and similar findings are reported for both sexes.

Animal protocols

TRIB3 knockout mice were a gift from Prof. Laurie J. Goodyear at the Joslin Diabetes Center, constructed as described previously (20). *Trib3*-floxp mice were purchased from GemPharmatech (strain no. T019128, C57BL/6JGpt-*Trib3em1Cflox*/Gpt). Homozygous *Trib3*-floxp mice were

crossed with SM22-Cre and Cdh5-Cre mice to generate smooth muscle cell -specific *TRIB3* knockout (SMC-*TRIB3*[KO]) and endothelial cell -specific *TRIB3* knockout (EC-*TRIB3*[KO]) mice, respectively. Homozygous *Trib3*-floxp mice served as controls for *TRIB3* knockout experiments. *ApoE* knockout and C57BL/6 mice were obtained from Vital River Lab Animal Technology Co., Ltd (Beijing, China).

Based on previous experience in our laboratory, which involved surgical procedures and late mortality, as well as inherent heterogeneity among the CKD models themselves, we initially planned to include 25 animals in each experimental group to ensure the statistical significance and robustness of the findings. The inclusion and exclusion criteria for enrollment and endpoints were predefined. The inclusion criteria were all surviving mice that received treatment were included in the study. Mice that did not survive until the end of the study were excluded (Supplementary Table 6).

The animals were kept in polycarbonate cages in rooms with controlled temperature and humidity, on a 12-hour light/dark cycle. They were provided with standard chow and tap water ad libitum.

Aortic artery samples from *db/db* and *ApoE* knockout mice administered STZ were provided by Qiming Deng and Ranran Qin (Affiliated Cardiovascular Hospital of Qingdao University). The experimental procedure is illustrated in Supplementary Figure 11.

UUO CKD and 5/6 nephrotomy procedure were performed as previously described (43). Eight-week-old C57BL/6 mice underwent 7 d of right ureteral obstruction with a non-traumatic titanium microvascular clip for 7 days, followed by the release of this obstruction. After 7 days of recovery, reversal of the obstruction was confirmed by the resolution of hydronephrosis, and

the contralateral left kidney was ligated and excised. The sham mice underwent surgical manipulation without ureteral obstruction or nephrectomy. In the 5/6 nephrotomy, the right kidney of 8 weeks old C57BL/6 mice was exposed through a flank incision and removed, and the stump was ligated with a 4-0 silk wire. One week later, the left kidney was exposed, and the upper and lower poles were resected through a lateral incision. All group mice were subjected to euthanasia by overdose phenobarbital in 15 weeks old ($\geq$150 mg/kg, i.p.).

For CKD after AKI, a 2-step procedure was used as previously described (44). The operation was performed under isoflurane anesthesia (1.5%–2%). In summary, the right kidney was subjected to cortical electrocautery via a 2 cm incision on the flank, followed by left total nephrectomy through a similar incision after a period of 2 weeks. Control animals underwent sham operations, which involved the removal of the capsule from both kidneys. For metabolic CKD, nephrectomy was performed in the right kidney of 6-week-old ApoE-knockout mice. The mice were provided a high-fat diet (HFD; 20% fat, 20% sugar, and 1.25% cholesterol) for a duration of 6 weeks. When the mice reached 12 weeks of age, they were injected once with low-dose STZ (75–80 mg/kg i.p.). The model mice exhibited hyperglycemia, IR, and glucose intolerance, as previously described (23, 45). Littermate WT mice underwent a similar sham operation and were injected once with the same volume of saline for 12 weeks. The sham mice were provided a standard laboratory diet with normal phosphate (0.5%), while the CKD mice received a high-phosphate (1.5%) diet for 12 weeks. *TRIB3* knockout and CTR mice were injected subcutaneously with 6 $\times 10^5$ IU/kg of vitamin D_3 daily for three days for Vitamin D_3-induced vascular calcification model. A micellar solution prepared by mixing ethanol, cremophor, and water was used as the solvent. All group mice were subjected to euthanasia by overdose

21

phenobarbital in 24 weeks old (≥150 mg/kg, i.p.).

Blood pressure and pulse wave velocity (PWV) Measurements

At the end of the experiment, the mice were anesthetized with 1–2% isoflurane, and a Millar

Mikro-tip 1.4F pressure transducer (SPR-839, Millar Instruments, Houston, Texas, USA) was

inserted into the right carotid artery to measure arterial blood pressure. Ultrasound detectors

(Vevo 2100, MX400, EKV imaging) focused on the abdominal aorta or femoral artery to measure

the pulse wave propagation distance. The PWV was determined by dividing the distance by the

time interval between the pressure wavefronts (46).

Renal function parameters

Serum creatinine and blood urea nitrogen (BUN) levels were measured spectrophotometrically

(C011-2-1 and C013-1-1, Nanjing Jiancheng Bioengineering Institute) using commercial kits

according to the manufacturer's instructions (46).

Human arteries samples

Human coronary arteries were obtained from cadavers. Carotid plaque samples were obtained via

endarterectomy. The source of the samples and patient characteristics have been thoroughly

described previously (47). Samples of renal arteries were obtained from receptors and donors in

renal transplantation. In accordance with the principles of the Declaration of Helsinki, the

Research Ethics Committee of Shandong University approved the study after informed consent

was obtained from the patients or their authorized representatives. The clinical characteristics of

the serum donors are listed in Supplementary Table 4-6.

Cell culture

Primary human aortic smooth muscle cells (hVSMC) were commercially obtained from ScienCell

Research Laboratories (CA, USA) and maintained in smooth muscle cell medium (SMCM) at 37°C in a 5% CO2 environment. Only cells from passages 4 to 6 were utilized for the experiments. Human HEK293T cells were obtained from KeyGene BioTech (China) and cultured in Dulbecco's Modified Eagle's medium (DMEM) supplemented with 10% fetal bovine serum (FBS, Gibco).

Primary mVSMC were isolated from the mouse aorta and cultured in SMCM as described previously (48). Only cells from passages 3 to 5 were utilized for the experiments.

Plasmids and RNA interference

Cells were transfected with 2 μg DNA encoding constitutively Smurf1 in pcDNA3.1 vector, or empty vector as control using Lipofectamine 3000 reagent (Invitrogen, USA) according to the manufacturer's protocol. Following transfection, cells were incubated for 24 hours for fluorescence microscopy, 48 hours for luciferase assay and western blotting, and 7 days for calcification experiments.

HVSMC and HEK293 cells were transfected with 10 nM shRNA or 10 nM negative control (NC) using Lipofectamine 3000 reagent.

The sequences of shRNAs with higher silencing efficiency are as follows: human TRIB3 sequences: sense 5'-CACCGCATCTTGCTGTGAAGAATAACGAATTATTCTTCACAGCAAGATGC-3', antisense

5'- AAAAGCATCTTGCTGTGAAGAATAATTCGTTATTCTTCACAGCAAGATGC -3',

human ATF4 sequences: sense 5'-CCGGCATGATCCCTCAGTGCATAAACTCGAGTTTATGCACTGAGGGATCATGTTTTT

G-3' , antisense 5'-AATTCAAAAACATGATCCCTCAGTGCATAAACTCGAGTTTATGCACTGAGGGATCATG-3' , human CHOP sequences: sense 5'-CCGGCTGCACCAAGCATGAACAATTCTCGAGAATTGTTCATGCTTGGTGCAGTTTTTG-3', antisense 5'-AATTCAAAAACTGCACCAAGCATGAACAATTCTCGAGAATTGTTCATGCTTGGTGCAG-3', mouse ATF4 sequences: sense 5'-CACCGCTGCTTACATTACTCTAATCCGAAGATTAGAGTAATGTAAGCAGC -3', antisense 5'-AAAAGCTGCTTACATTACTCTAATCTTCGGATTAGAGTAATGTAAGCAGC -3', mouse CHOP sequences: sense 5'-CACCGCTCTCCAGATTCCAGTCAGACGAATCTGACTGGAATCTGGAGAGC -3', antisense 5'-AAAAGCTCTCCAGATTCCAGTCAGATTCGTCTGACTGGAATCTGGAGAGC -3'.

In vitro VSMC calcification

As previously described, VSMC calcification was induced for 1 week in osteogenic medium containing 2.6 mmol/L Pi. Calcification was quantified by alizarin red staining or by measuring the total calcium content in the cell lysates using the MTB method with a Calcium Assay Kit (C004-2-1, Nanjing Jiancheng Bioengineering Institute). After 48 hours of incubation following transfection, silencing efficiency was assessed by reverse transcription quantitative polymerase chain reaction (RT-qPCR). ALPL activity was measured after 7 days of silencing, and calcium deposition was assessed after 14 days of silencing

Aortic calcification

Calcium deposits in aortic sections were stained using Alizarin red (Sigma Aldrich) and Von Koss, as described previously (49). ImageJ software (NIH Bethesda, MD, USA) was used to quantify the percentage of positively stained areas in each section.

Aortic stiffness measurements ex vivo

After euthanizing the mice with isoflurane anesthesia and cervical dislocation, the abdominal aorta was harvested. The isolated aorta was promptly transferred to a pre-cold, oxygenated physiological salt solution (PSS). Each ring was placed between two stainless steel wires of a Small Vessel Myograph (DMT 610M, Danish Myo Technology). Wall tension was measured by incrementally increasing the distance (stretch length) between the wires in 50 μm steps, and the measurements were recorded for a duration of 2 min per aorta after each increment in stretch length (50).

E3 ubiquitin ligase prediction

UbiBrowser 2.0 (51) is used to predict and visualize ubiquitin ligase (E3)/deubiquitinase (DUB) substrate interactions. The Likelihood Ratio was showed by bubble size and Confidence Score was present by color depth in matrix bubble diagram.

Multiple sequence alignment (MSA) and ubiquitination sites prediction

Further identification of a sequence similarity between species for Smurf1 was assessed using multiple sequence alignment (MSA) derived from eight orthologous proteins, including human, gorilla, macac, mouse, rat, cow, pig, and clawed frogs. The ubiquitination sites of Smurf1 were predicted using UbiNet 2.0 (52).

Human and mouse RNA Sequencing and enrichment analysis

Total RNA from hVSMC and mVSMC from NC siRNA and *siTRIB3* transfected, *TRIB3* knockout, and littermate mice was obtained. After extracting the total RNA, the samples were subjected to agarose gel electrophoresis, Nanodrop quality assessment, and quantification. For mRNA enrichment, oligo (dT) magnetic beads were used (for degraded RNA or prokaryotic samples, rRNA removal kits were used directly). RNA-sequencing libraries were constructed using a kit that involved RNA fragmentation, randomly primed reverse transcription to generate first-strand cDNA, synthesis of second-strand cDNA using dUTP, end repair of double-stranded cDNA with A-tailing, and ligation of the Illumina adapter for sequencing. The final library was amplified using PCR. The constructed libraries were quality checked using an Agilent 2100 Bioanalyzer, and library quantification was performed using qPCR. Sequencing was performed on an Illumina HiSeq 4000 sequencer. Gene- and transcript-level fragments per kilobase of transcript per million mapped reads (FPKM) were calculated using BallGown. Differential expression analysis was conducted separately at the gene and transcript levels to identify genes or transcripts that showed significant differences in expression between the groups. We cross-ranked the 1610 upregulated and 1356 downregulated genes using a dataset of 257 genes associated with VC (DisGenNet C0342649, https://www.disgenet.org/browser/0/1/0/C0342649/). The differentially expressed genes were subjected to clustering analysis, GO functional enrichment analysis, and pathway enrichment analysis to further explore their biological relevance using KangChen Biotech's customized Python software.

Transcription factor binding signature analysis

Down-regulated DEG were uploaded to KnockTF2.0 (25) for transcription factor enrichment analysis. Fifty-five transcription factors were listed after the set (FDR-adjusted) *p*-value of 0.05.

The enriched transcription factors overlapped with vascular calcification-associated 257 genes（DisGenNet C0342649), which were visualized using Eveen (53).

RT-qPCR

The expression of *TRIB3* and osteogenic factors in the aortic tissues and VSMC was determined using RT-qPCR. Total RNA was extracted using TRIzol (Invitrogen) and reversely transcribed into cDNA. RT-qPCR was performed using specific primers as shown in Supplementary Table 7. The $2^{-\Delta\Delta Ct}$ method was used for comparisons. The relative mRNA levels were normalized to those of GAPDH.

The enzyme-linked immunosorbent assay (ELISA)

After centrifugation of the thawed human tissue homogenate, the supernatant was collected and the target protein concentration was measured using a commercially available Human TRIB3 ELISA kit (EH2519, FineTest, China). The total protein concentration, determined by the BCA assay, was used for normalization.

Reagents and antibodies

Cycloheximide and MG132 were purchased from MCE (USA). Tunicamycin 4-phenylbutyric acid (4PBA) and phosphate were purchased from Sigma-Aldrich (USA). Protein A/G agarose gels were obtained from Santa Cruz Biotechnology (USA). The antibodies used were shown in Supplementary Table 8.

Western blot analysis

Western blot analysis is performed as described previously (48). Total protein were extracted from vascular tissue and from cells by using the RIPA lysis supplemented with a protease inhibitor (P1005, Beyotime, China). Proteins were run on 10% SDS-polyacrylamide gel

electrophoresis (SDS-PAGE) and transferred to 0.22 μm PVDF membrane. Each membrane was blocked by 5% BSA (Albumin from bovine serum) and incubated with primary antibodies overnight at 4°C. Bound antibodies were detected by horseradish peroxidase–conjugated secondary antibody (1:5000) and visualized by a chemiluminescent reagent (WBKLS0500, Millipore, Germany). For detection, a chemiluminescence instrument (GE, Amersham Imager 680) was employed.

Co-immunoprecipitation and immunoblot analysis

For immunoblot analysis, cells or tissues were lysed with RIPA. Protein concentrations were quantified using a BCA Protein Assay Kit, and the concentrations of different samples were adjusted to equal levels using the extraction reagent. For immunoprecipitation (IP), whole-cell extracts were lysed in IP buffer (150 mM saline, 50 mM Tris–HCl, 1% NP-40, pH 7.8, and mammalian cell-specific protease inhibitor cocktail (Merck, Darmstadt, Germany) and proteins were quantified using the BCA assay. After centrifugation for 10 min at 13,000g, supernatants were collected and incubated with protein A/G Plus–Agarose immunoprecipitation reagent (Santa Cruz Biotechnology, USA) together with 1 μg of the corresponding antibodies for 4°C incubations overnight. The beads were washed, and immunoprecipitated proteins were eluted from beads by 2x loading buffer and then were incubated at 100°C for 5 min. Immunoprecipitated proteins were subjected to western blot analysis.

Immunofluorescence microscopy

HVSMC cells were transfected with the expression plasmid for *TRIB3*, Smurf1 WT and Smurf1ΔC2 on glass coverslips. After 48 h of transfection, cells were fixed with 4% paraformaldehyde, permeabilized with 0.1% Triton X-100, and blocked with 1% bovine serum

albumin for 30 min at room temperature. Next, fixed cells were incubated with the indicated primary antibodies overnight at 4°C. Detection was performed by incubating with fluorescent dye-conjugated secondary antibodies. Nuclei were counterstained with DAPI (Sigma-Aldrich, USA). A leica microscope was used for imaging.

Immunohistochemistry (IHC) and immunofluorescence (IF)

The slides were subjected to dewaxing and antigen retrieval using citrate buffer (pH 6.0). Subsequently, they were treated with 3% H_2O_2, followed by blocking with 5% BSA for 30 minutes at 37°C. The slides were then incubated with primary antibodies overnight at 4°C. Negative controls consisting of isotype IgG antibodies were included. The next day, horseradish peroxidase-conjugated secondary antibodies or fluorescein coupling secondary antibodies were applied for 0.5 h at room temperature in IHC. Color development was performed using a DAB kit (ZSGB-Bio, Beijing, China) for IHC. Hematoxylin or DAPI was used to counterstain the nuclei in the IHC or IF staining process.

Ubiquitination assay

To analyze the ubiquitination of Myc–TRIB3, HA expressing HA-ubiquitin (WT), HA–ubiquitin (K48), HA–ubiquitin (K63) and Flag–Smurf1(WT) or its mutants were used to transfect HEK293T cells, and then whole-cell extracts were immunoprecipitated with the Myc-specific antibody and analyzed by western blotting with an anti-HA antibody. For analysis of ubiquitination of Smurf1, VSMC were stimulated with phosphate.

Luciferase Reporter Assays

To create a wild-type luciferase construct, we inserted a DNA fragment from the mouse *TRIB3* promoter into a pGL3Basic vector (Promega, Madison, WI, USA). Mutant constructs specifically

targeting the predicted ATF4 and CHOP sites in the *TRIB3* promoter were generated by site-directed mutagenesis (Promega).

For the luciferase assay, a luciferase reporter plasmid was transfected into mVSMC cultured in 24-well plates using Lipofectamine 3000. To ensure accurate measurements, we co-transfected the pRL-TK plasmid, which carries Renilla luciferase under the control of the thymidine kinase promoter, as an internal control to monitor transfection efficiency.

Following transfection, cells were exposed to 2.6 mM concentration of Pi for 24 h. Luciferase activity was subsequently assessed using a Dual-Luciferase Assay Kit (Promega).

Chromatin Immunoprecipitation (ChIP) Assay

Human primary VSMC infected with 2.6 mM Pi underwent the following procedure: initially, they were incubated with 1% formaldehyde for 10 min to facilitate the cross-linking of DNA-protein complexes, which were then halted with 0.125 mol/L glycine. The cells were harvested, lysed, and sonicated to generate genomic DNA fragments ranging from 300 to 1000 bp in length. The lysates were subsequently exposed to 2 μg of anti-ATF4, anti-CHOP, or normal IgG antibody and left to incubate overnight at 4°C. Protein A/G plus-agarose beads (Santa Cruz CA Biotechnology) saturated with single-stranded salmon sperm DNA were added to the lysates and incubated for 2 h. The resulting immunocomplexes were washed and eluted. Then immunocomplexes were add 1uL DNase-free RNaseA and incubate for 30 min at 37°C. The cross-linked DNA was released by incubating the immunocomplexes with proteinase K buffer at 65°C. This DNA was further purified using the phenol/chloroform/isoamyl alcohol method and subsequently amplified by PCR using *TRIB3* promoter-specific primers.

FAIRE (Formaldehyde-Assisted Isolation of Regulatory Elements) PCR Assay

30

After cross-linked DNA were released from immunocomplexes with proteinase K, collect sample by brief centrifugation with a microfuge and resuspended with 200 μL 10 mM Tris-HCl pH 7.4 to a final volume of 300 μL. Then the sample was vortex for 10 min after adding 300 μL phenol/chloroform/isoamyl alcohol. DNA with an open chromatin region in the aqueous layer (top) was transferred and repeatedly washed with phenol/chloroform/isoamyl alcohol. The final DNA product were precipitated with 1/10 volume 3 M Sodium Acetate (pH 5.2), 2 volumes 95% ethanol, and 1 μL 20 mg/mL glycogen. Then the DNA was subsequently amplified by PCR with *TRIB3* promoter and 5UTR and 3UTR-specific primers (54).

Molecular dynamics simulation for protein-protein interaction

Human Smurf1 (UniProt accession: Q9HCE7) and TRIB3 (UniProt accession: Q96RU7) structures were predicted using the AlphaFold 2 (55). The dynamics simulation was conducted using the Gromacs 2022.3(56). The simulation was performed under static conditions at 300 K and atmospheric pressure (1 bar). The force field employed was Amber99sb-ildn and the solvent used was a water molecule (Tip3p water model). The molecular dynamics simulation system was subjected to energy minimization using the steepest descent method. Subsequently, it underwent 100,000 steps of NVT (canonical ensemble) equilibration and 100,000 steps of NPT (isothermal-isobaric ensemble) equilibration with a coupling constant of 0.1 ps and a duration of 100 ps. Finally, a production molecular dynamics simulation was conducted, comprising 5,000,000 steps with a time step of 2 fs, resulting in a cumulative simulation time of 100 ns. After completing the simulation, a t-test was performed using the built-in software tools to calculate the root mean square deviation (RMSD), root mean square fluctuation (RMSF), and protein radius of gyration for each amino acid movement trajectory. Additionally, the free energy (MMPBSA), free-energy

landscape, and other relevant data were computed.

Surface Plasmon Resonance (SPR)

Recombinant Smurf1 protein was immobilized on a CM5 sensor chip using an Amine Coupling Kit (BR100050). TRIB3 protein was applied at concentrations ranging from 31 nM to 8 μM, resulting in a kinetic affinity constant (KD) of 12.8 nM. Protein-protein interactions were analyzed using the Biacore T200 system, and surface plasmon resonance (SPR) signals were processed and fitted using the kinetics model in Biacore T200 Evaluation Software to calculate the KD value.

Statistics

Data are presented as scatter dot plots with the mean ± SEM (standard error of the mean). The number of independent biological samples (n) and experimental repeats provided in both the figures and their corresponding figure legends. The normality of the data was evaluated using the Shapiro-Wilk test. In cases where the data did not follow a normal distribution, appropriate transformations (such as logarithmic, reciprocal, or square root) were applied to achieve normality, as determined using the Shapiro-Wilk test. Statistical analysis was conducted using 2-tailed Student t test for normal distribution with homogeneous variances, unpaired 2-tailed Student t test incorporating Welch correction in scenarios of heterogeneity in variances and the Mann-Whitney U test for non-normally distributed data in two independent groups. For datasets with more than two independent groups and a single factor, 1-way ANOVA followed by Tukey's test for homoscedastic data or the Games-Howell test for heteroscedastic data. Non-normal datasets were analyzed using the Steel-Dwass method. Data obtained from the time course were analyzed using repeated-measures ANOVA. Two-group comparisons were performed using unpaired 2-

tailed t-tests or U-tests. Correlations between the groups were evaluated using Pearson's correlation test. Statistical significance was set at $p< 0.05$. significant. All analyses were conducted using Graphpad Prism 8.0 software.

Study approval

The protocol for this clinical study conformed to the ethical guidelines of the 1975 Declaration of Helsinki and was approved by the Research Ethics Committee of Shandong University. All participants signed an informed consent form before participating in the study. Written informed consent was obtained from all participants. The experimental animal protocols complied with the Management Rules of the Chinese Ministry of Health and were approved by the Ethics Committee.

Data Availability

Published ATF4 and C/EBP homologous protein (CHOP) Chromatin Immunoprecipitation (ChIP)-seq data are available from the Gene Expression Omnibus (GSE35681). The transcriptome bulk sequence data have been deposited in the China National Center for Bioinformation (41, 42) (HRA013574). The study was approved by the QL IRB (12073).

(No.2020SDUCRCC027).

Reference

1. Ibels LS, Alfrey AC, Huffer WE, Craswell PW, Anderson JT, and Weil R, 3rd. Arterial calcification and pathology in uremic patients undergoing dialysis. *Am J Med.* 1979;66(5):790-6.

2. Raggi P, Boulay A, Chasan-Taber S, Amin N, Dillon M, Burke SK, et al. Cardiac calcification in adult hemodialysis patients. A link between end-stage renal disease and cardiovascular disease? *J Am Coll Cardiol.* 2002;39(4):695-701.

3. Stompór T. An overview of the pathophysiology of vascular calcification in chronic kidney disease. *Peritoneal dialysis international : journal of the International Society for Peritoneal Dialysis.* 2007;27 Suppl 2:S215-22.

4. Budoff MJ, Rader DJ, Reilly MP, Mohler ER, 3rd, Lash J, Yang W, et al. Relationship of estimated GFR and coronary artery calcification in the CRIC (Chronic Renal Insufficiency Cohort) Study. *Am J Kidney Dis.* 2011;58(4):519-26.

5. Kazancioğlu R. Risk factors for chronic kidney disease: an update. *Kidney International Supplements.* 2013;3:368-71.

6. Verberckmoes SC, Persy V, Behets GJ, Neven E, Hufkens A, Zebger-Gong H, et al. Uremia-related vascular calcification: More than apatite deposition. *Kidney International.* 2007;71:298-303.

7. Shroff R, Long DA, and Shanahan C. Mechanistic insights into vascular calcification in CKD. *J Am Soc Nephrol.* 2013;24(2):179-89.

8. Durham AL, Speer MY, Scatena M, Giachelli CM, and Shanahan CM. Role of smooth muscle cells in vascular calcification: implications in atherosclerosis and arterial stiffness. *Cardiovasc Res.* 2018;114(4):590-600.

9. Beamish JA, He P, Kottke-Marchant K, and Marchant RE. Molecular regulation of contractile smooth muscle cell phenotype: implications for vascular tissue engineering. *Tissue Eng Part B Rev.* 2010;16(5):467-91.

10. Schwarz DS, and Blower MD. The endoplasmic reticulum: structure, function and response to cellular signaling. *Cell Mol Life Sci.* 2016;73(1):79-94.

11. Ron D, and Walter P. Signal integration in the endoplasmic reticulum unfolded protein response. *Nat Rev Mol Cell Biol.* 2007;8(7):519-29.

12. Hetz C. The unfolded protein response: controlling cell fate decisions under ER stress and beyond. *Nature Reviews Molecular Cell Biology.* 2012;13:89-102.

13. Hotamisligil GS. Endoplasmic reticulum stress and the inflammatory basis of metabolic disease. *Cell.* 2010;140(6):900-17.

14. Cybulsky AV. Endoplasmic reticulum stress in proteinuric kidney disease. *Kidney Int.* 2010;77(3):187-93.

15. Mao C, Wang M, Luo B, Wey S, Dong D, Wesselschmidt R, et al. Targeted Mutation of the Mouse Grp94 Gene Disrupts Development and Perturbs Endoplasmic Reticulum Stress Signaling. *PLoS ONE.* 2010;5:e10852.

16. Zhuang A, and Forbes JM. Stress in the kidney is the road to pERdition: is endoplasmic reticulum stress a pathogenic mediator of diabetic nephropathy? *Journal of Endocrinology.* 2014;222:R97-R111.

17. Taniguchi M, and Yoshida H. Endoplasmic reticulum stress in kidney function and disease. *Current Opinion in Nephrology and Hypertension.* 2015;24:345-50.

18. Cybulsky AV. Endoplasmic reticulum stress, the unfolded protein response and autophagy in kidney diseases. *Nat Rev Nephrol.* 2017;13(11):681-96.

19. Furmanik M, van Gorp R, Whitehead M, Ahmad S, Bordoloi J, Kapustin A, et al. Endoplasmic Reticulum Stress Mediates Vascular Smooth Muscle Cell Calcification via Increased Release of Grp78 (Glucose-Regulated Protein, 78 kDa)-Loaded Extracellular Vesicles. *Arterioscler Thromb Vasc Biol.* 2021;41(2):898-914.

20. Koh HJ, Toyoda T, Didesch MM, Lee MY, Sleeman MW, Kulkarni RN, et al. Tribbles 3 mediates endoplasmic reticulum stress-induced insulin resistance in skeletal muscle. *Nat Commun.* 2013;4:1871.

21. Prudente S, Sesti G, Pandolfi A, Andreozzi F, Consoli A, and Trischitta V. The Mammalian Tribbles Homolog TRIB3, Glucose Homeostasis, and Cardiovascular Diseases. *Endocrine Reviews.* 2012;33(4):526-46.

22. Ti Y, Xie G-l, Wang Z-h, Bi X-l, Ding W-y, Wang J, et al. TRB3 Gene Silencing Alleviates Diabetic Cardiomyopathy in a Type 2 Diabetic Rat Model. *Diabetes.* 2011;60(11):2963-74.

23. Wang Z-h, Shang Y-y, Zhang S, Zhong M, Wang X-p, Deng J-t, et al. Silence of TRIB3 Suppresses Atherosclerosis and Stabilizes Plaques in Diabetic ApoE−/−/LDL Receptor−/− Mice. *Diabetes.* 2012;61(2):463-73.

24. Morse E, Schroth J, You Y-H, Pizzo DP, Okada S, RamachandraRao S, et al. TRB3 is stimulated in diabetic kidneys, regulated by the ER stress marker CHOP, and is a suppressor of podocyte MCP-1. *American Journal of Physiology-Renal Physiology.* 2010;299(5):F965-F72.

25. Feng C, Song C, Liu Y, Qian F, Gao Y, Ning Z, et al. KnockTF: a comprehensive human gene expression profile database with knockdown/knockout of transcription factors. *Nucleic Acids Research.* 2020;48(D1):D93-D100.

26. Yang Q, Zhao J, Chen D, and Wang Y. E3 ubiquitin ligases: styles, structures and functions. *Molecular Biomedicine.* 2021;2:23.

27. Fu L, Cui CP, Zhang X, and Zhang L. The functions and regulation of Smurfs in cancers. *Semin Cancer Biol.* 2020;67(Pt 2):102-16.

28. Chan MC, Nguyen PH, Davis BN, Ohoka N, Hayashi H, Du K, et al. A novel regulatory mechanism of the bone morphogenetic protein (BMP) signaling pathway involving the carboxyl-terminal tail domain of BMP type II receptor. *Mol Cell Biol.* 2007;27(16):5776-89.

29. Richmond L, and Keeshan K. Pseudokinases: a tribble-edged sword. *Febs j.* 2020;287(19):4170-82.

30. Lu K, Li P, Zhang M, Xing G, Li X, Zhou W, et al. Pivotal role of the C2 domain of the Smurf1 ubiquitin ligase in substrate selection. *J Biol Chem.* 2011;286(19):16861-70.

31. Du K, Herzig S, Kulkarni RN, and Montminy M. TRB3: a tribbles homolog that inhibits Akt/PKB activation by insulin in liver. *Science.* 2003;300(5625):1574-7.

32. Hua F, Mu R, Liu J, Xue J, Wang Z, Lin H, et al. TRB3 interacts with SMAD3 promoting tumor cell migration and invasion. *J Cell Sci.* 2011;124(Pt 19):3235-46.

33. Hayakawa M. Role of K63-linked polyubiquitination in NF-κB signalling: which ligase catalyzes and what molecule is targeted? *J Biochem.* 2012;151(2):115-8.

34. Dong L, Liu L, Li Y, Li W, Zhou L, and Xia Q. E3 ligase Smurf1 protects against misfolded SOD1 in neuronal cells by promoting its K63 ubiquitylation and aggresome formation. *Hum Mol Genet.* 2022;31(12):2035-48.

35. Franco LH, Nair VR, Scharn CR, Xavier RJ, Torrealba JR, Shiloh MU, et al. The Ubiquitin Ligase Smurf1 Functions in Selective Autophagy of Mycobacterium tuberculosis and Anti-tuberculous Host Defense. *Cell Host Microbe.* 2017;21(1):59-72.

36. Sluimer J, and Distel B. Regulating the human HECT E3 ligases. *Cell Mol Life Sci.* 2018;75(17):3121-41.

37. Scott JL, Frick CT, Johnson KA, Liu H, Yong SS, Varney AG, et al. Molecular Analysis of Membrane Targeting by the C2 Domain of the E3 Ubiquitin Ligase Smurf1. *Biomolecules.* 2020;10(2).

38. Fei C, Li Z, Li C, Chen Y, Chen Z, He X, et al. Smurf1-mediated Lys29-linked nonproteolytic polyubiquitination of axin negatively regulates Wnt/β-catenin signaling. *Mol Cell Biol.* 2013;33(20):4095-105.

39. Chen H, Ghori-Javed FY, Rashid H, Adhami MD, Serra R, Gutierrez SE, et al. Runx2 Regulates Endochondral Ossification Through Control of Chondrocyte Proliferation and Differentiation. *Journal of Bone and Mineral Research.* 2014;29:2653-65.

40. Lin JH, Walter P, and Yen TSB. Endoplasmic Reticulum Stress in Disease Pathogenesis. *Annual Review of Pathology: Mechanisms of Disease.* 2008;3:399-425.

41. Database Resources of the National Genomics Data Center, China National Center for Bioinformation in 2023. *Nucleic Acids Res.* 2023;51(D1):D18-d28.

42. Chen T, Chen X, Zhang S, Zhu J, Tang B, Wang A, et al. The Genome Sequence Archive Family: Toward Explosive Data Growth and Diverse Data Types. *Genomics Proteomics Bioinformatics.* 2021.

43. Martínez-Klimova E, Aparicio-Trejo OE, Tapia E, and Pedraza-Chaverri J. Unilateral Ureteral Obstruction as a Model to Investigate Fibrosis-Attenuating Treatments. *Biomolecules.* 2019;9(4).

44. Gagnon RF, and Duguid WP. A reproducible model for chronic renal failure in the mouse. *Urol Res.* 1983;11(1):11-4.

45. Li Y, Yan H, Wang F, Huang S, Zhang Y, Wang Z, et al. Activation of EphA1-Epha receptor axis attenuates diabetic nephropathy in mice. *Biochemical and biophysical research communications.* 2017;486(3):693-9.

46. Ma C, Chen T, Ti Y, Yang Y, Qi Y, Zhang C, et al. Ranolazine alleviates contrast-associated acute kidney injury through modulation of calcium independent oxidative stress and apoptosis. *Life Sci.* 2021;267:118920.

47. Sun T, Wang F, He Y, Mao B, Han M, Liu H, et al. Enlarged Pericarotid Lymph Nodes Suggest Recent Ischemic Symptoms in Patients with Carotid Atherosclerosis. *Front Immunol.* 2022;13:900642.

48. Li Y, Qin R, Yan H, Wang F, Huang S, Zhang Y, et al. Inhibition of vascular smooth muscle cells premature senescence with rutin attenuates and stabilizes diabetic

atherosclerosis. *J Nutr Biochem.* 2018;51:91-8.

49.   Voelkl J, Luong TT, Tuffaha R, Musculus K, Auer T, Lian X, et al. SGK1 induces vascular smooth muscle cell calcification through NF-κB signaling. *J Clin Invest.* 2018;128(7):3024-40.

50.   Jin L, Lipinski A, and Conklin DJ. A Simple Method for Normalization of Aortic Contractility. *J Vasc Res.* 2018;55(3):177-86.

51.   Wang X, Li Y, He M, Kong X, Jiang P, Liu X, et al. UbiBrowser 2.0: a comprehensive resource for proteome-wide known and predicted ubiquitin ligase/deubiquitinase-substrate interactions in eukaryotic species. *Nucleic Acids Res.* 2022;50(D1):D719-d28.

52.   Li Z, Chen S, Jhong JH, Pang Y, Huang KY, Li S, et al. UbiNet 2.0: a verified, classified, annotated and updated database of E3 ubiquitin ligase-substrate interactions. *Database (Oxford).* 2021;2021.

53.   Yang M, Chen T, Liu YX, and Huang L. Visualizing set relationships: EVenn's comprehensive approach to Venn diagrams. *Imeta.* 2024;3(3):e184.

54.   Giresi PG, Kim J, McDaniell RM, Iyer VR, and Lieb JD. FAIRE (Formaldehyde-Assisted Isolation of Regulatory Elements) isolates active regulatory elements from human chromatin. *Genome Res.* 2007;17(6):877-85.

55.   Tunyasuvunakool K, Adler J, Wu Z, Green T, Zielinski M, Žídek A, et al. Highly accurate protein structure prediction for the human proteome. *Nature.* 2021;596(7873):590-6.

56.   Van Der Spoel D, Lindahl E, Hess B, Groenhof G, Mark AE, and Berendsen HJ. GROMACS: fast, flexible, and free. *J Comput Chem.* 2005;26(16):1701-18.
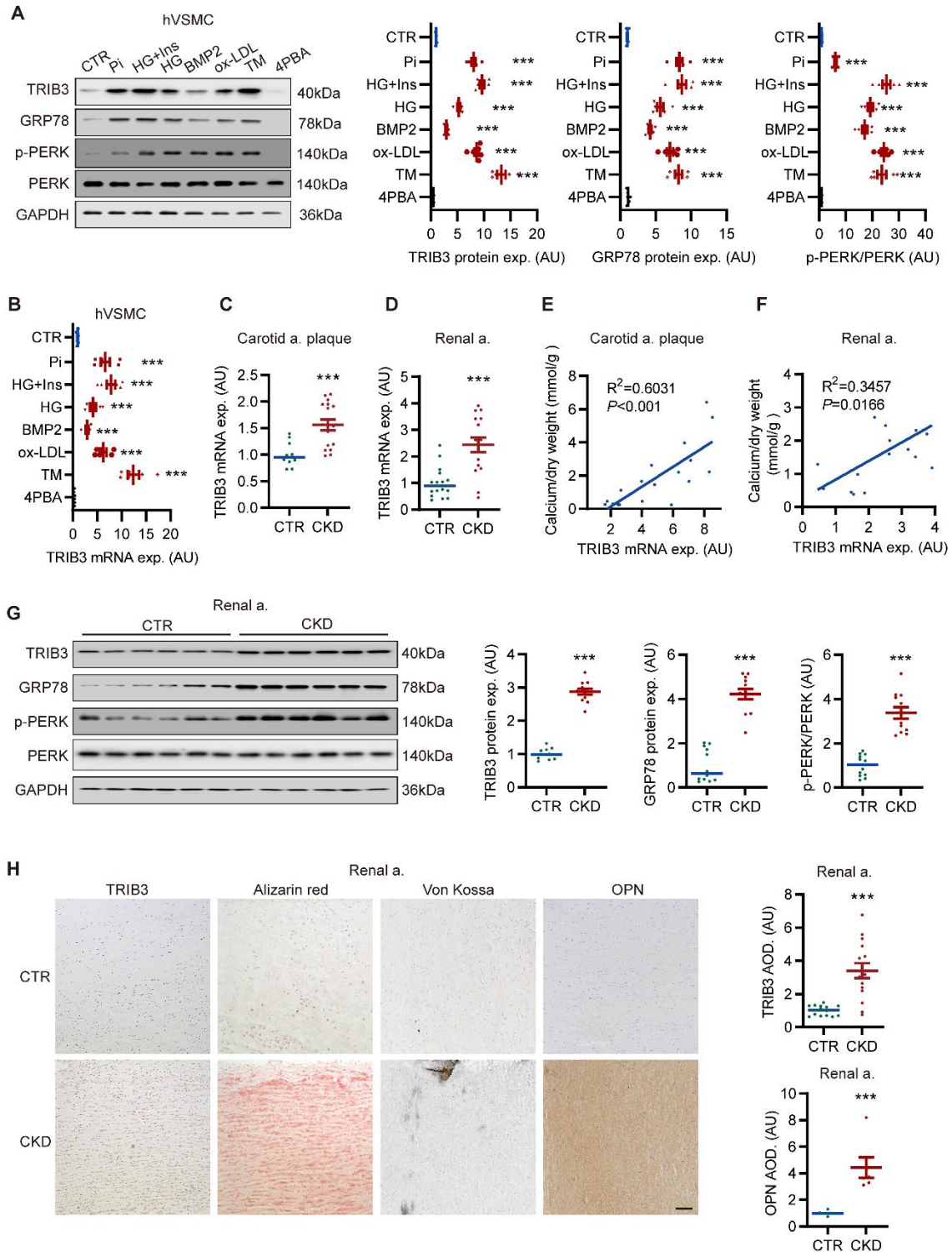
Figure and figure legends

Figure 1. Elevated VSMCs TRIB3 expression in ER stress.

A, Representative western blots and analysis of TRIB3, GPR78 and phosphorylation of PERK expression in primary hVSMC following treatment with L-glucose osmotic medium control (CTR) or 2.6 mM phosphate (Pi), 25mM glucose plus 10 nM Insulin (HG+Ins), 25 mM glucose (HG), 10 nM human bone morphogenetic protein 2 (BMP2), 80 μg/mL ox-LDL, 0.1 μg/ml tunicamycin, 5 μM 4-Phenylbutyric acid (4PBA), n=6 per group. Quantification of the protein expression of TRIB3, GPR78 and phosphorylation of PERK. Statistical analyses were performed using the 1-way ANOVA. Relative values are compared against those of the CTR group. **B**, RT-qPCR analysis of TRIB3 relative mRNA expression in hVSMCs following indicated treatment. n=6 per group. Statistical analyses were performed using the 1-way ANOVA. Relative values are compared against those of the CTR group. **C-D**, RT-qPCR analysis of TRIB3 relative mRNA expression in chronic kidney disease (CKD) patients' carotid artery and renal artery, n=10-17 per group. Statistical analyses were performed using the unpaired 2-tailed Student *t* test with Welch correction. Relative values are compared against those of CTR group. **E-F**, Correlation of TRIB3 relative mRNA expression and calcium deposition in carotid artery and renal artery plaque tissue from CTR and CKD patients, *P* represents the 2-tailed probability value of the Pearson correlation, n=18 per group. **G**, Representative western blots and analysis of TRIB3, GPR78 and PERK protein expression in renal artery from CKD patients and individuals with normal renal function (n=12 in each). Statistical analyses were performed using the unpaired 2-tailed Student *t* test with Welch correction. Relative values are compared against those of the CTR group. **H**, Representative original histological images and immunohistochemistry (IHC) analysis showing TRIB3 expression and ectopic calcification in renal artery from control CTR and CKD patients (n=15 per group). Alizarin Red staining identifies mid-to-late-stage mineralization, Von Kossa

staining identifies late-stage calcification, osteopontin (OPN) (n=6 per group) serves as a marker for osteogenic differentiation. Statistical analyses were performed using the unpaired 2-tailed Student t test with Welch correction. Relative values are compared against those of the CTR group. Scale bar=100 µm. Scatter dot plots and arithmetic means ± SEM (arbitrary units (AU)). ***$P <$ 0.001 statistically significant $vs.$ CTR.
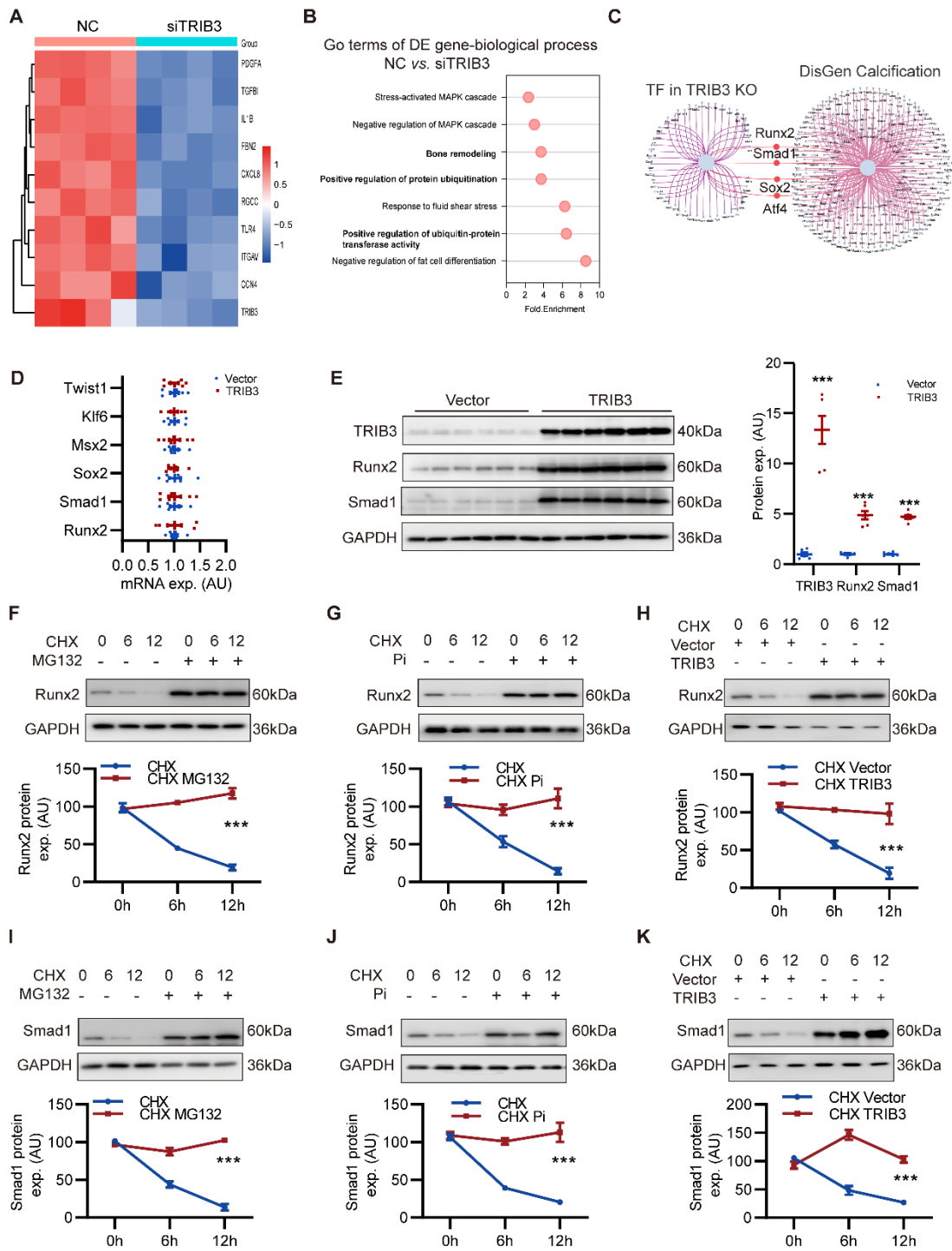
Figure 2. TRIB3 Suppresses Runx2 and Smad1 Degradation in VSMC

A, Heatmap of differentially expressed genes（DEGs）of vascular calcification phenotype gene

cluster (DisGenNet C0342649) in hVSMC transfected with negative control (NC) or siTRIB3. **B,**

Gene Ontology (GO) analysis of DEGs in hVSMCs transfected with NC or siTRIB3. **C,** The

overlap of transcription factor (TF) binding signature analysis for DEG after TRIB3 knockout and DisGenNet C0342649. **D,** RT-qPCR analysis of osteogenic TF (Runx2, Smad1, Sox2, Msx2, Klf6 and Twist1) mRNA expression in hVSMCs transfected with blank vector (Vector) and TRIB3 overexpression adenovirus (TRIB3). n=6 per group. Statistical analyses were performed using the unpaired 2-tailed Student t test. Relative values are compared against those of the Vector group. **E,** Representative western blots and analysis of protein expression in TRIB3, Runx2, Smad1 in hVSMCs transfected with Vector and TRIB3, n=6 per group. Statistical analyses were performed using the unpaired 2-tailed Student t test. Relative values are compared against those of the Vector group. ***$P < 0.001$ statistically significant *vs.* Vector. **F-K,** Representative western blots and analysis of Runx2 (F-H) and Smad1(I-K) protein expression in hVSMCs following treatment with or without MG132 (10μM, 4 h), Pi (2.6 mM, 48h), Vector or TRIB3 (48h) and then incubated with CHX (50 μg/mL) for indicated time points. n=6 per group. cycloheximide (CHX). Statistical analyses were performed using the repeated measures two-way ANOVA. Scatter dot plots and arithmetic means ± SEM (AU). ***$P < 0.001$ statistically significant *vs.* CHX or CHX Vector.
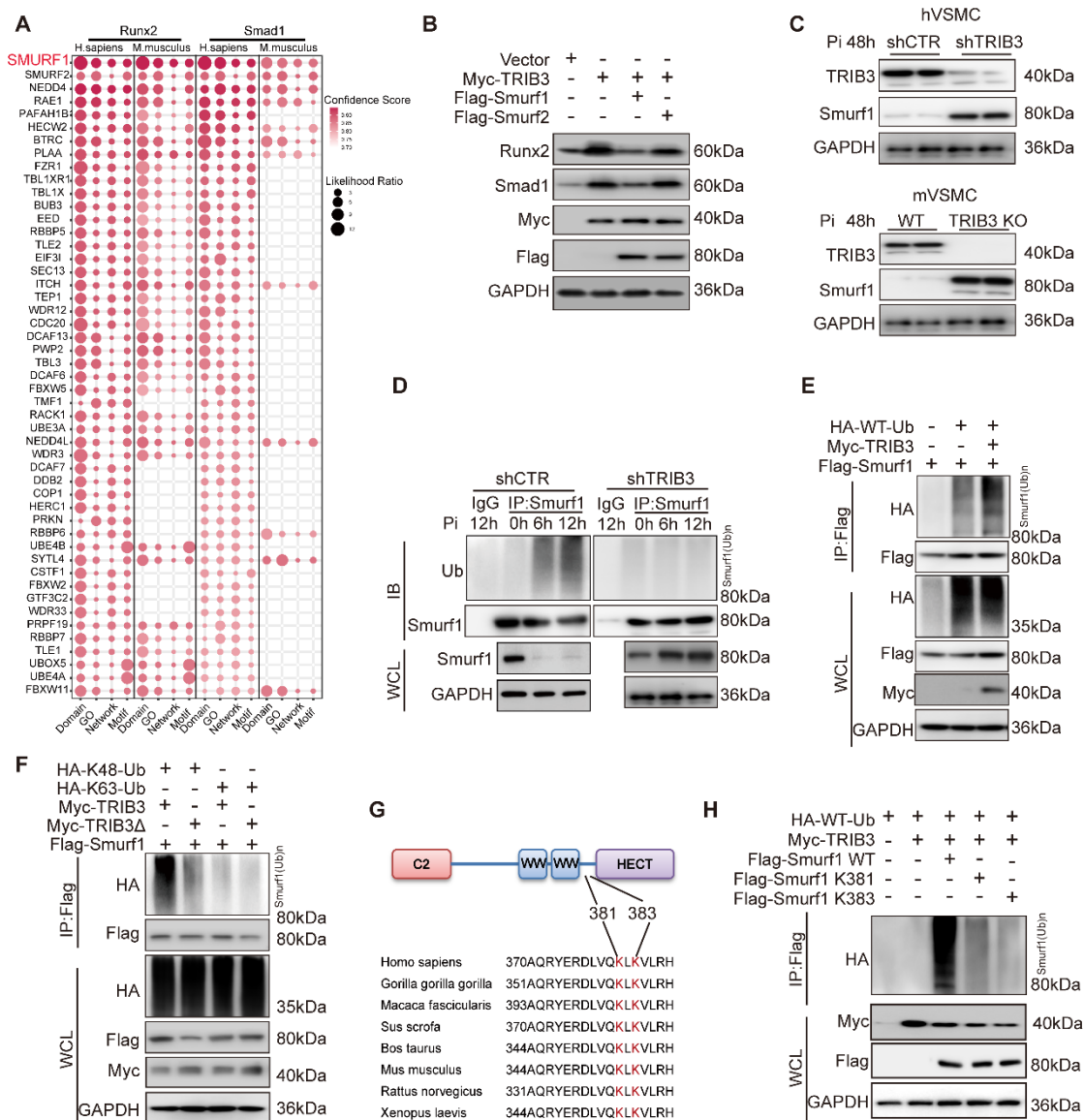
Figure 3. TRIB3 Promotes Runx2 and Smad1 Ubiquitination via Interacting with Smurf1

A, Matrix bubble diagram of E3 ubiquitin ligases prediction of Runx2 and Smad1 in human and mouse. **B**, Representative western blots of protein expression in Runx2 and Smad1 in hVSMC transfected with exogenous TRIB3, Smurf1 and Smurf2 plasmid. The presented results represent one of three independent replicates. **C**, Representative western blots of protein expression in TRIB3 and Smurf1 in hVSMC and mVSMC treated with Pi (2.6 mM, 48h). The presented results represent one of three independent replicates. **D**, Representative western blots of ubiquitination of Smurf1 in hVSMC transfected with shTRIB3 and stimulated with treated with Pi (2.6 mM) at the indicated times. The presented results represent one of three independent replicates. **E**, Representative western blots of ubiquitination of exogenous Smurf1 in HEK293T cells. The

presented results represent one of three independent replicates. **F**, Representative western blots of ubiquitination of exogenous Smurf1 in HEK293T cells transfected with plasmids encoding mutant of TRIB3 238-266aa (TRIB3Δ)，HA-ubiquitin (K48) and HA-ubiquitin (K63). The presented results represent one of three independent replicates. **G**, The multiple sequence alignment and K48 ubiquitin site prediction for Smurf1. **H**, Representative western blots of Smurf1 ubiquitination assay with exogenous Smurf1 (Smurf1 WT), Smurf1 mutant with the lysine residue replaced by arginine in K381 (K381R) and K383 (K383R). The presented results represent one of three independent replicates.
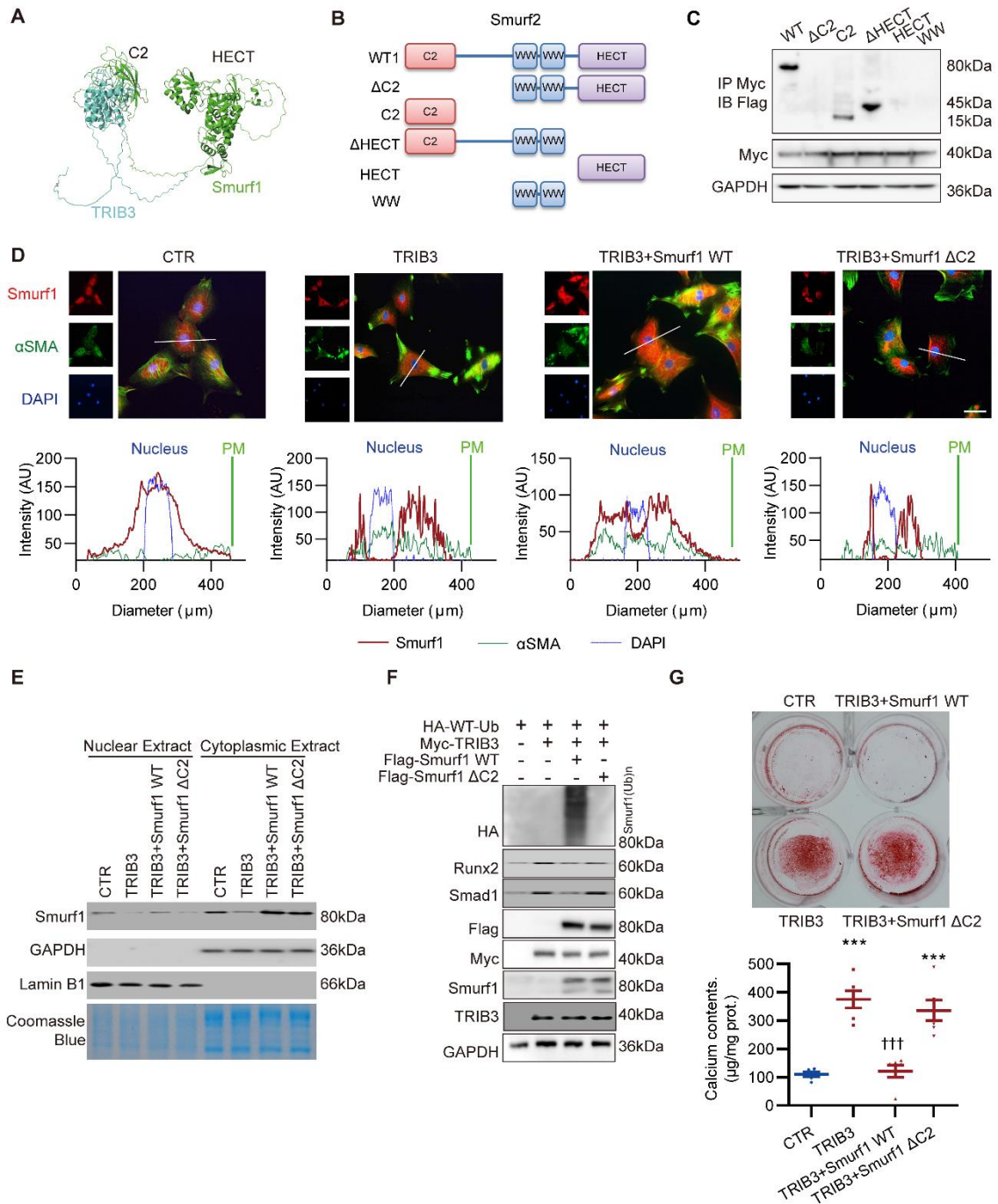
Figure 4. TRIB3 interacted Smurf1 and promoted its self ubiquitination through C2 domain

A, Structure docking to simulate the interaction between Smurf1 and TRIB3. **B,** Smurf1 domain structure and deletion mutants used in the study (WT, ΔC2, C2, ΔHECT, HECT, and WW). **C,** Representative IP western blots of Myc-TRIB3 and Flag-Smurf1 and mutants in HEK293T cells were transfected with plasmid for 48h. The presented results represent one of three independent replicates. **D,** Representative immunofluorescence of Smurf1 and αSMA in hVSMC were

transfected with TRIB3, Smurf1 WT and Smurf1ΔC2 for 48h. The 4',6-diamidino-2-phenylindole (DAPI) indicated the nuclei, and the margin of αSMA indicated the plasma membrane (PM). The white line is the path of the colocalization analysis. Scale bar=20 μm. The presented results represent one of three independent replicates. **E,** Representative western blots of cellular fractionation showing Smurf1 expression in the nuclear and cytoplasmic fractions in hVSMC. The presented results represent one of three independent replicates. **F,** Representative western blots of ubiquitination of exogenous Smurf1, Smurf1ΔC2 with TRIB3 in HEK293T cells. The presented results represent one of three independent replicates. **G,** Representative Alizarin red staining of hVSMC transfected with plasmids encoding mutant of Smurf1, Smurf1ΔC2 and TRIB3, then treated with Pi (2.6 mM) for 7 days (n=6 in each). The calcium contents analysis of hVSMC transfected with plasmids encoding mutant of Smurf1, Smurf1ΔC2 and TRIB3, then treated with Pi (2.6 mM) for 7 days. Statistical analyses were performed using the 2-way ANOVA. Relative values are compared against those of the CTR group. ***$P < 0.001$ statistically significant *vs.* CTR. †††$P < 0.001$ statistically significant *vs.* TRIB3. Each experiment was repeated independently for a minimum three times. Scatter dot plots and arithmetic means ± SEM (AU).
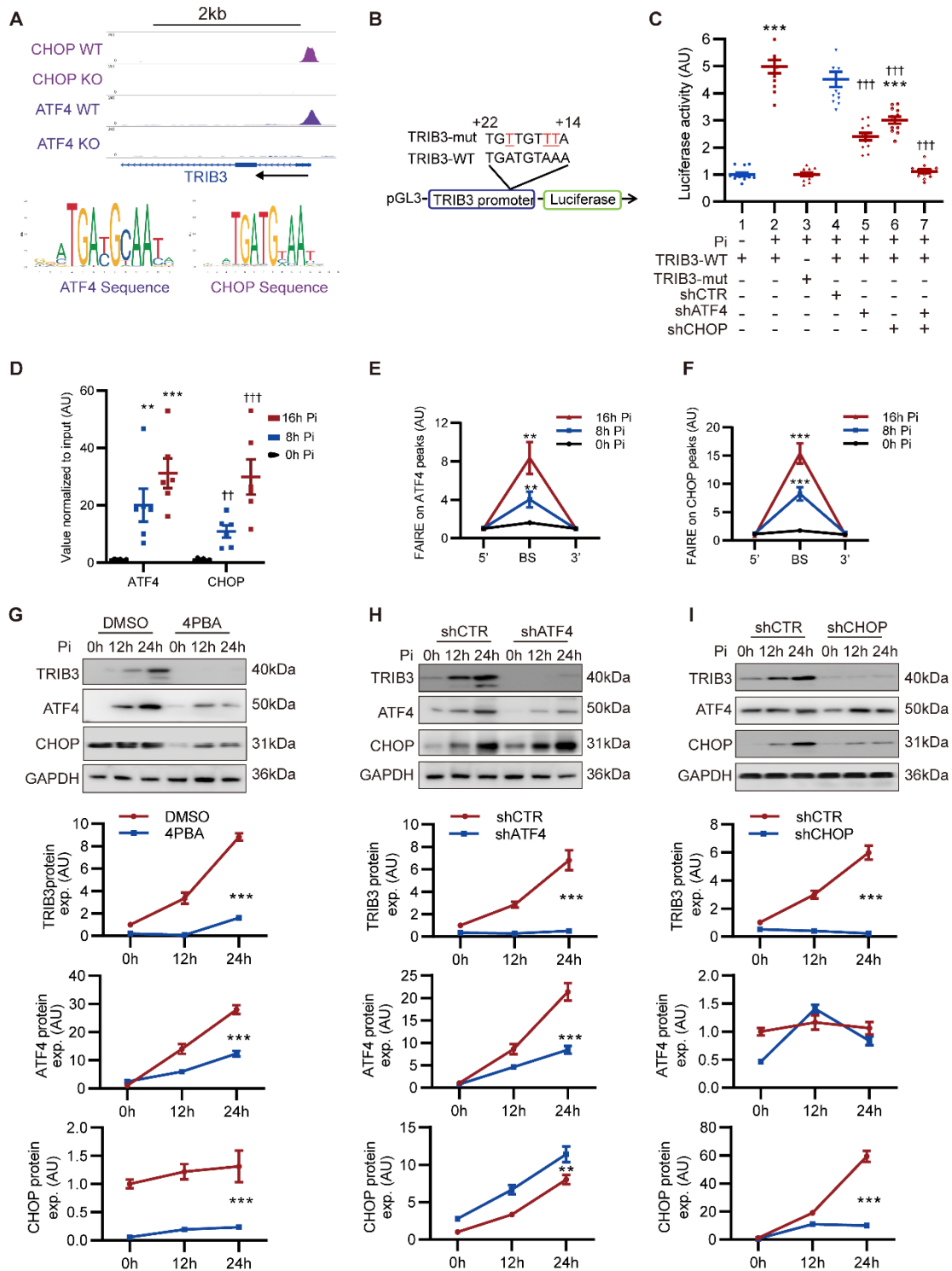
Figure 5. ATF4 and CHOP induced TRIB3 transcription in phosphorate stimuli

A, IGV browser displayed for the TRIB3 loci displaying ChIP-seq tracks and sequence logo for

ATF4 and CHOP. **B,** Wild-type or mutant TRIB3 promoter luciferase plasmid. **C,** Luciferase

activity of mVSMC transfected with TRIB3-WT or TRIB3-mut promoter luciferase plasmid

(Treated Pi (2.6 mM) 12h, or transfected with shRNA for knockdown ATF4 and CHOP for 48h). Statistical analyses were performed using the 2-way ANOVA. ***$P < 0.001$ statistically significant *vs*. 1.TRIB3-WT without Pi treatment, †††$P < 0.001$ statistically significant *vs*. 4.transfected with shCTR and TRIB3-WT with Pi treatment. **D,** ChIP-PCR showing enrichment of both ATF4 and CHOP at the TRIB3 binding site (BS) in mVSMC treated Pi (2.6 mM) for 24h. Statistical analyses were performed using the 1-way ANOVA. **$P < 0.01$, ***$P < 0.001$ statistically significant *vs*. 0h Pi treatment (ATF4), ††$P < 0.01$, †††$P < 0.001$ statistically significant *vs*. 0h Pi treatment (CHOP). **E-F,** Formaldehyde-Assisted Isolation of Regulatory Elements (FAIRE)-ChIP PCR was performed on Pi (2.6 mM) for indicated time in mVSMC. Statistical analyses were performed using the repeated measures two-way ANOVA. **G-I,** Representative western blots of TRIB3, ATF4, and CHOP in mVSMC stimulated with treated with Pi (2.6 mM) at the indicated times after pretreated with 4PBA 5 μM for 12h, or transfected with shRNA for knockdown ATF4 and CHOP for 48h. Statistical analyses were performed using the repeated measures two-way ANOVA. Scatter dot plots and arithmetic means ± SEM (AU). *$P < 0.05$, **$P < 0.01$, ***$P < 0.001$ statistically significant *vs*. 0h treatment, DMSO, or shCTR. Each experiment was repeated independently for three to six times. Scatter dot plots and arithmetic means ± SEM (AU).
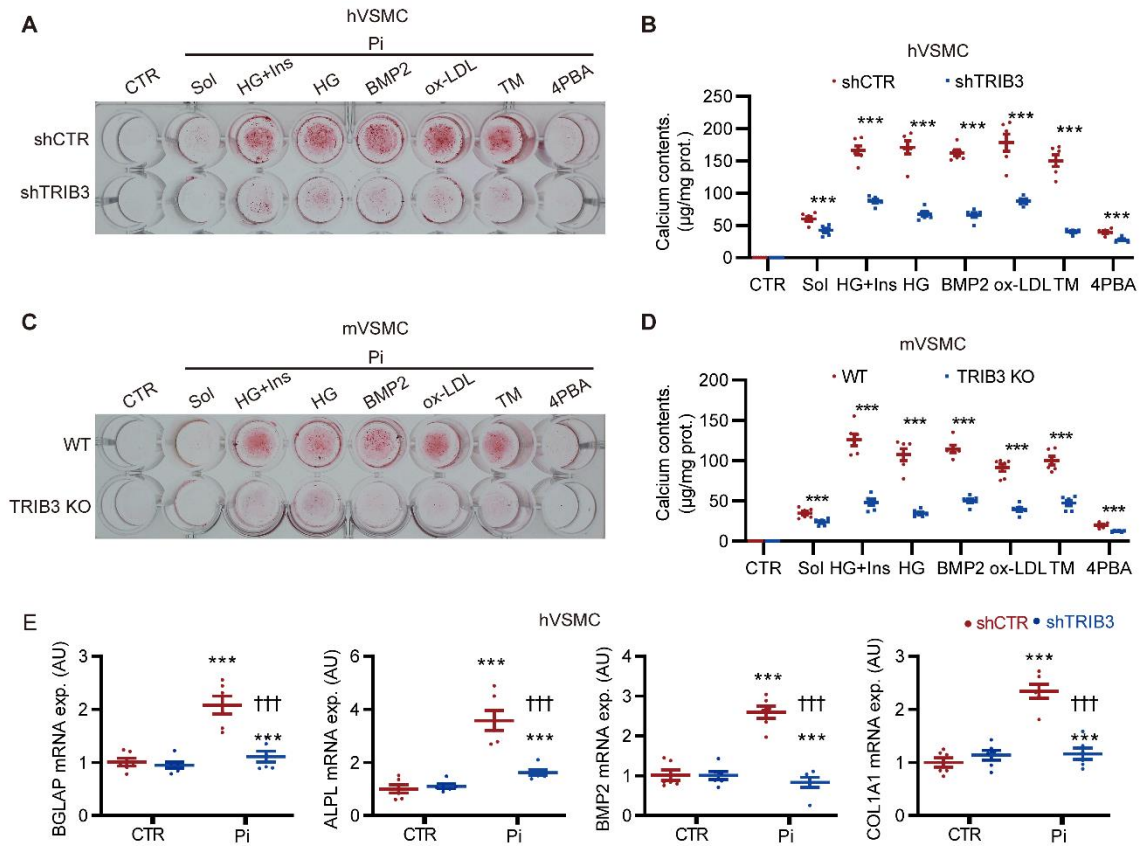
Figure 6 Effect of TRIB3 deficiency on ER-induced osteogenic transdifferentiation of primary aortic smooth muscle cells

A, Representative Alizarin red staining of hVSMC transfected with shCTR and shTRIB3 plasmids, then stimulated with treated with L-glucose osmotic medium control (CTR), solvent (Sol), 2.6 mM Pi plus 25mM HG plus 10nM Ins, 25mM HG, 10nM BMP2, 80 μg/mL ox-LDL, 0.1 μg/ml TM or 5μM 4PBA for 7 days. **B,** Calcium content analysis for A (n=6 in each). Statistical analyses were performed using the 1-way ANOVA. Relative values are compared against those of the CTR group. **C,** Representative Alizarin red staining of mVSMC from WT and TRIB3 knockout (KO) mice, then stimulated with treated with 2.6 mM Pi plus 25mM HG plus 10nM Ins, 25mM HG, 10nM BMP2, 80 μg/mL ox-LDL, 0.1 μg/ml TM or 5μM 4PBA for 7 days. **D,** Calcium content analysis for C (n=6 in each). Statistical analyses were performed using

49

the 1-way ANOVA. Relative values are compared against those of the CTR group. **E,** RT-qPCR

analysis of osteogenic factor (BGLAP, ALPL, BMP2, and COL1A1) mRNA expression in

transfected with shCTR and shTRIB3 plasmids, then stimulated with treated with Pi (2.6 mM, 7d)

(n=6 in each). Statistical analyses were performed using the 2-way ANOVA. $***P < 0.001$

statistically significant *vs.* CTR or Sol. †††$P < 0.001$ statistically significant *vs.* Pi plus shCTR.

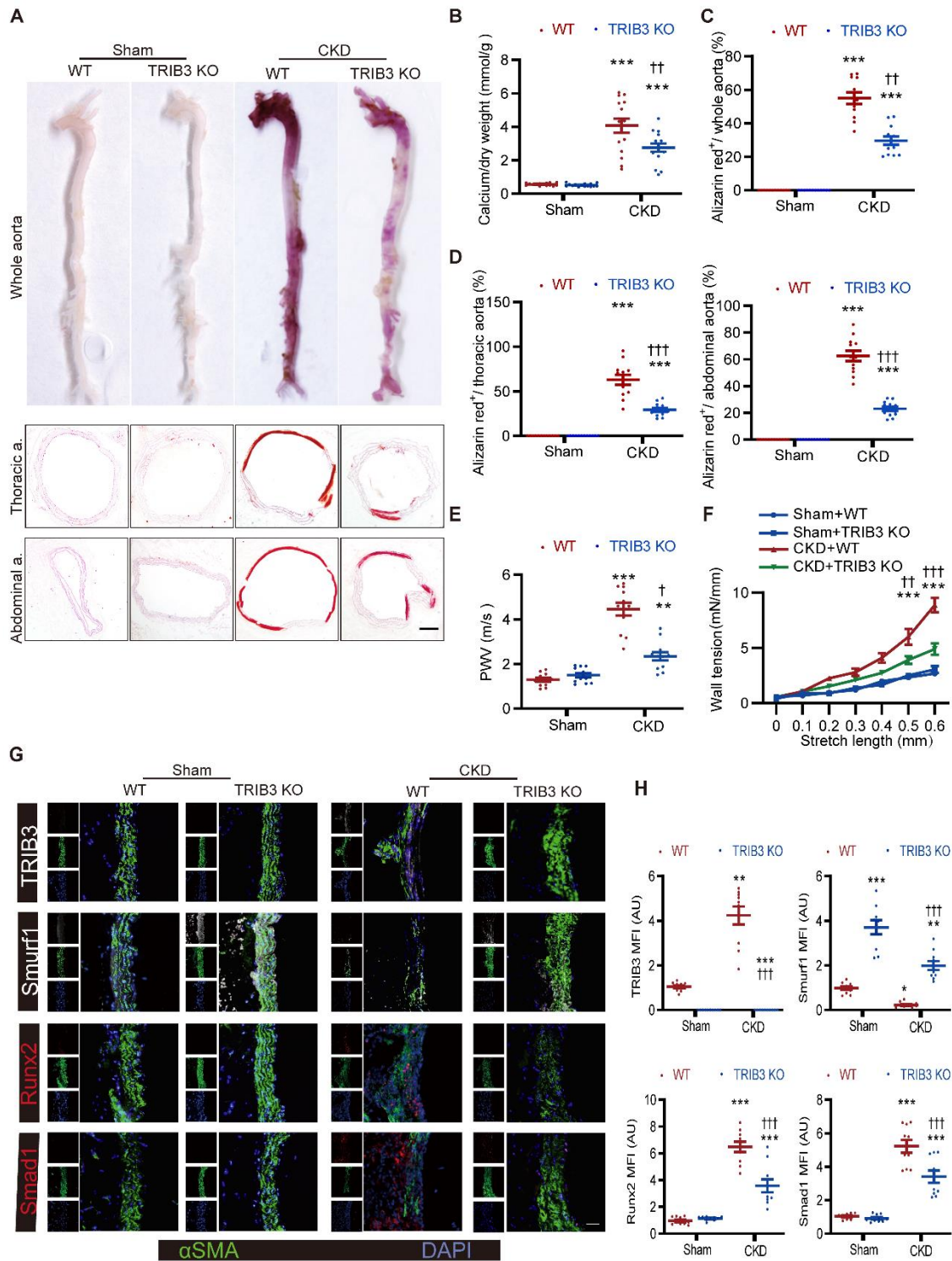Scatter dot plots and arithmetic means ± SEM (AU).

Figure 7. Effect of TRIB3 deficiency during AKI–induced CKD vascular calcification in mice.

A, Representative Alizarin red staining of whole aorta, thoracic and abdominal aorta section images showing aortic alizarin red staining in Acute kidney injury (AKI)-induced CKD mice.

Scale bar: 100μm. Calcified areas are shown as red staining. **B,** Calcium content analysis in the aortic arch of AKI-induced CKD mice, normalized by dry weight. Statistical analyses were performed using the 2-way ANOVA. **C-D**, The ratio of Alizarin Red-positive area to the whole aortic area, thoracic aorta, and abdominal aorta in the indicated group of mice (n=12 in each). Statistical analyses were performed using the 2-way ANOVA. **E,** Abdominal aortic pulse wave velocity (PWV) in AKI-induced CKD mice (n=12 in each). Statistical analyses were performed using the 2-way ANOVA. **F,** Wall tension (n = 3 rings, 6 mice per group; mN/mm) during mechanical stretch (mm) ex vivo of abdominal aorta isolated from AKI-induced CKD mice. **G,** Representative immunofluorescence of TRIB3, Smurf1, Runx2 and Smad1 in thoracic aortic tissue of AKI-induced CKD mice. Scale bar: 50μm. **H,** The quantitative analysis for G (n=5 incontinuous sections from 10 mice per group). Statistical analyses were performed using the 2-way ANOVA. **$P < 0.01$, ***$P < 0.001$ statistically significant *vs.* Sham WT mice; †$P < 0.05$, ††$P < 0.01$, †††$P < 0.001$ statistically significant *vs.* CKD WT mice. n =15 per group unless otherwise indicated. Scatter dot plots and arithmetic means ± SEM (AU).
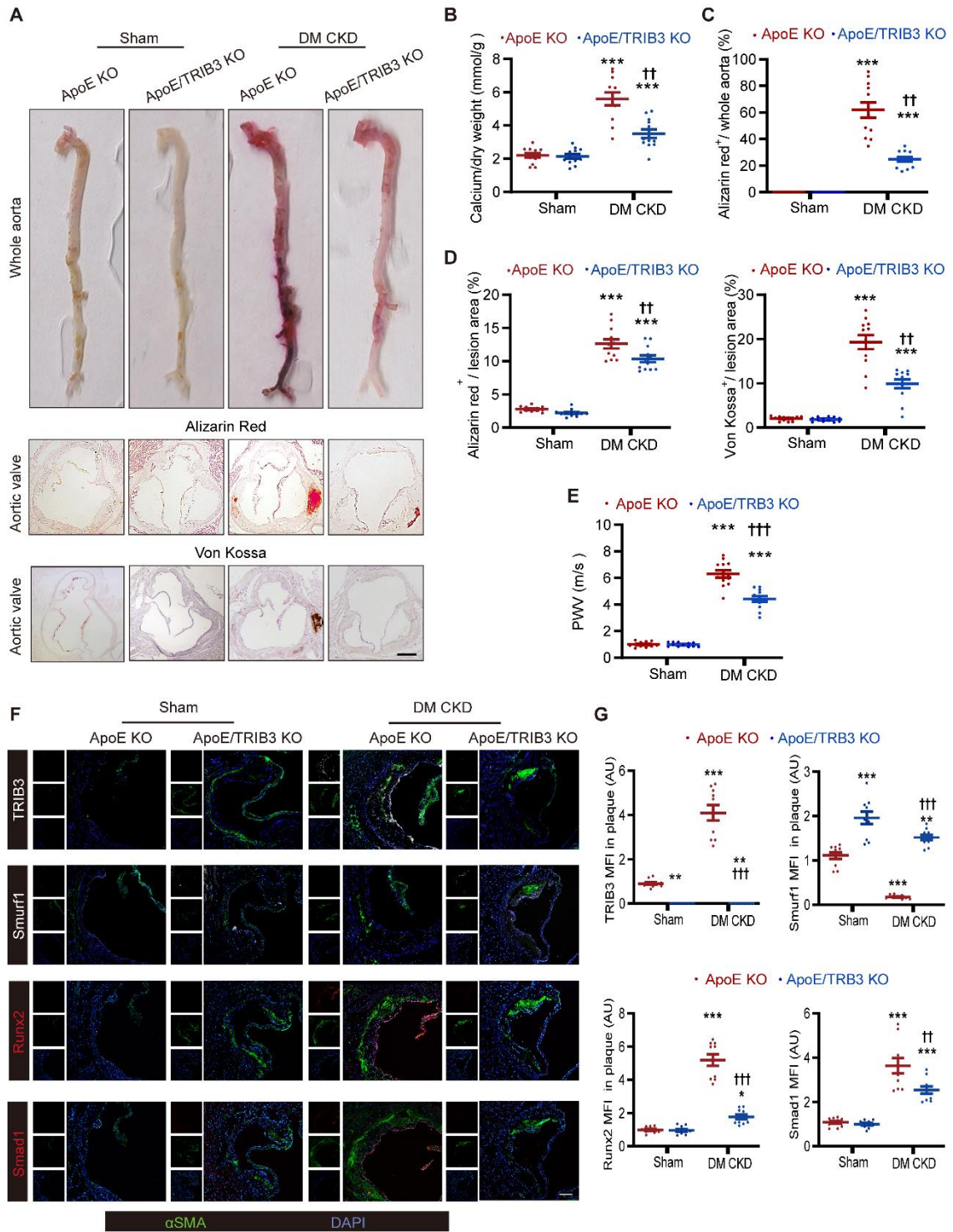
Figure 8. Effect of TRIB3 deficiency during metabolic CKD induced vascular calcification in mice

A, Representative Alizarin red staining of whole aorta images, Alizarin red staining of aortic valve section, Von Kossa staining of aortic valve section in metabolic CKD mice. Scale bar:

100μm. Calcified areas are shown as red staining. **B,** Calcium content analysis in the aortic arch of metabolic CKD mice, normalized by dry weight. **C,** The area ratio of calcification to the whole aortic area in metabolic CKD mice. Statistical analyses were performed using the 2-way ANOVA. **D**, The ratio of Alizarin Red-positive and Von Kossa-positive area to the whole aortic valves (sections with max valve plaque lesion area). Statistical analyses were performed using the 2-way ANOVA. **E,** PWV in metabolic CKD mice. Statistical analyses were performed using the 2-way ANOVA. **F,** Representative immunofluorescence of TRIB3, Smurf1, Runx2 and Smad1 in thoracic aortic tissue of metabolic CKD mice. **G,** The quantitative analysis for F (n=5 incontinuous sections from 10 mice per group). Statistical analyses were performed using the 2-way ANOVA.　**P* < 0.01, ***P* < 0.001 statistically significant *vs.* Sham ApoE KO mice; ††*P* < 0.01, †††*P* < 0.001 statistically significant *vs.* DM ApoE KO mice. n=12 per group unless otherwise indicated. Scatter dot plots and arithmetic means ± SEM (AU).